Remote Sensing of Environment 140 (2014) 241–256

Contents lists available at ScienceDirect

Remote Sensing of Environment

journal homepage: www.elsevier.com/locate/rse

Evaluation of six satellite-derived Fraction of Absorbed Photosynthetic Active Radiation (FAPAR) products across the Australian continent

Christopher A. Pickett-Heaps [a,*], Josep G. Canadell [a], Peter R. Briggs [a], Nadine Gobron [b], Vanessa Haverd [a], Matt J. Paget [a], Bernard Pinty [b], Michael R. Raupach [a]

[a] CSIRO Marine and Atmospheric Research, GPO Box 3023, Canberra, ACT 2601, Australia
[b] European Commission, DG Joint Research Centre, Institute for Environment and Sustainability, Climate Risk Management Unit, Ispra, Italy

ARTICLE INFO

Article history:
Received 30 April 2013
Received in revised form 23 August 2013
Accepted 24 August 2013
Available online xxxx

Keywords:
FAPAR
Vegetation spatio-temporal dynamics
Satellite product evaluation & inter-comparison
In-situ comparison and evaluation
Validation
Australia

ABSTRACT

Satellite remote sensing products of the Fraction of Absorbed Photosynthetically Active Radiation (FAPAR) are routinely used for diverse applications in Earth-System and land-surface modelling and monitoring. The availability of numerous products creates a need to understand the level of consistency between products, and reasons for inconsistencies. We evaluate the consistency of six FAPAR products (MODIS, MERIS, SeaWIFS, MODIS-TIP, SPOT-VEG, and AVHRR) across the Australian continent, using multi-year records. We find that seemingly large differences in FAPAR products over much of Australia can be explained by a simple offset present in certain products. Additional inconsistencies arise from different sensitivities in FAPAR to changes in vegetation cover. These inconsistencies can in turn be partially attributed to changes in biome type that are relevant to certain products and related model-specific assumptions.

The satellite FAPAR products are compared to ~800 observation-based estimates of fractional vegetation cover at field sites across Australia. After accounting for offsets in FAPAR, relatively high agreement occurs at sites classified as grasslands, shrublands and managed land (agriculture). Significant disagreement occurs at sites correctly classified as forests. Consequently, some products show significant differences in FAPAR between regions of similar vegetation cover but different biome classification. We find that all products show a much lower sensitivity to fractional vegetation cover (range in coefficient of linear regression: 0.28–0.61) than is predicted theoretically (0.96–1.18) using a canopy radiative transfer model. Reasons for this discrepancy are discussed.

1. Introduction

The Fraction of Absorbed Photosynthetically Active Radiation (FAPAR) is defined as the fraction of Photosynthetically Active Radiation (PAR) absorbed by green elements of healthy vegetation (FAO, 2008; Liang, Li, & Wang, 2012). Absorption of PAR occurs during photosynthesis and is closely related to leaf chlorophyll content (Gitelson, Gritz, & Merzlyak, 2003) and carbon assimilation (Sellers, 1985, 1987; Sellers, Berry, Collatz, Field, & Hall, 1992). FAPAR is an 'integrated indicator' of the status of the vegetation canopy (Gobron, Pinty, Taberner, et al., 2006) and is classified as an essential climate variable of the Earth (GCOS, 2006).

FAPAR is a physical quantity of the land-surface radiation budget and is defined as (Liang et al., 2012):

$$FADAR = \frac{PAR(\downarrow, TOC) - PAR(\downarrow, BOC) + PAR(\uparrow, BOC) - PAR(\uparrow, TOC)}{PAR(\downarrow, TOC)} \quad (1)$$

$\downarrow$	Downward radiation flux
$\uparrow$	Upward radiation flux
TOC	Top of canopy radiation
BOC	Bottom of canopy radiation

Advances in modelling the radiation and energy budget (e.g. Bacour, Baret, Beal, Weiss, & Pavageau, 2006; Gobron, Pinty, Verstraete, & Widlowski, 2000; Knyazikhin, Martonchik, Myneni, Diner, & Running, 1998; Pinty et al., 2007) that gives rise to observed spectral characteristics of the land surface have led to the definition of physically-based parameters that in turn describe the current state of healthy vegetation. Vegetation indices, such as the Normalized Difference Vegetation Index (NDVI) and the Enhanced Vegetation Index (EVI), are used to empirically diagnose the current state of vegetation and act as proxies for FAPAR (Donohue, McVicar, & Roderick, 2009; Liang et al., 2012; Myneni & Williams, 1994; Pinty, Lavergne, Widlowski, Gobron, & Verstraete, 2009). Leaf Area Index (LAI), a key land-surface parameter related to vegetation biomass and canopy structure, is a physically-based parameter and an intrinsic characteristic of the land surface (Pinty, Andredakis, et al., 2011). By contrast, FAPAR is a component of the land-surface radiation budget, and is estimated following its closure.

* Corresponding author.
E-mail address: christopher.pickett-heaps@csiro.au (C.A. Pickett-Heaps).

0034-4257/$ – see front matter © 2013 Elsevier Inc. All rights reserved.
http://dx.doi.org/10.1016/j.rse.2013.08.037

Satellite remote sensing has thus revolutionised our ability to characterise and monitor vegetation dynamics on a global scale. In combination with terrestrial land-surface models (Haverd et al., 2013; Jung et al., 2008; Kaminski et al., 2012; Knorr et al., 2010; Seixas, Carvalhais, Nunes, & Benali, 2009; Sellers et al., 1997), remote sensing can be used to constrain or otherwise inform the spatio-temporal dynamics of vegetation cover and better understand terrestrial carbon and water cycles. However, different satellite products show considerable disagreement (McCallum et al., 2010; Meroni et al., 2012; Seixas et al., 2009). These differences are due to several factors, including variations in the specific definition of FAPAR (such as whether a FAPAR estimate pertains to direct or indirect radiation).

Differences between products raise questions about the sensitivity of land-surface models to inconsistencies between products. For instance, McCallum et al. (2010) compared four FAPAR products over northern Eurasia. The highest level of inconsistency across the products occurred within the dominant vegetation type of mixed forests and needle-leaf forests. Improved consistency was observed within deciduous broadleaf forest and cropland. Meroni et al. (2012) evaluated three SPOT-VEGETATION based FAPAR products in three separate regions of contrasting bio-climatic characteristics (SW Brazil, northern Niger and southern France). The three products, using different algorithms, exhibited generally low to moderate agreement.

Seixas et al. (2009) compared the Moderate Resolution Imaging Spectroradiometer (MODIS) and MEdium Resolution Imaging Spectrometer (MERIS) FAPAR products over the Iberian Peninsula for 2003. MERIS routinely underestimated FAPAR and displayed greater spatial homogeneity than MODIS, despite high agreement in NDVI from both products. Consistent with McCallum et al. (2010), FAPAR agreement was somewhat dependent on biome type. Following parameter retuning of the Carnegie–Ames–Stanford Approach (CASA) model (Field, Randerson, & Malmström, 1995; Potter et al., 1993) for each satellite product, Seixas et al. (2009) identified reasonable agreement in site-based Net Primary Production (NPP)/Net Ecosystem Exchange (NEE) estimates, but a remaining discrepancy in seasonality was identified. Haverd et al. (2013) used two FAPAR products derived from MODIS and the Advanced Very High Resolution Radiometer (AHVRR) (Donohue, Roderick, & McVicar, 2008, data available at http://data.auscover.org.au) to drive a terrestrial land-surface model over Australia from 1990–2010. Despite parameter retuning of the land-surface model for each FAPAR product (resulting in highly consistent continental mean estimates of NPP), regional differences in NPP of up to 15% were identified. Seasonal discrepancies in FAPAR were identified as a key contributor to seasonal discrepancies in NPP.

The objectives of this paper are (1) to assess the degree of consistency of six global satellite FAPAR products across the Australian continent, using three geographical classifications based on drainage units and vegetation types; and (2) to identify where and why the products are inconsistent. The satellite FAPAR products are further evaluated against ~800 in-situ estimates of vegetation fractional cover (spatial scale ~100 m × 100 m) at ~600 field sites across Australia.

2. Data & methods

This section is divided into three main sub-sections: 2.1. Study Area, 2.2. Datasets and 2.3. Methods.

2.1. Study region: bio-climatic characteristics of Australia

Australia is the driest inhabited continent. Mean annual rainfall (1990–2011) is 493 mm.a^{-1} (61% of the global average, Haverd et al., 2013), with much of central Australia receiving <250 mm.a^{-1}. Annual runoff is ~70 mm.a^{-1} (or 14% of precipitation, Haverd et al., 2013), highlighting high rates of evapotranspiration. Northern Australia has a tropical dry, monsoonal climate. Climate zones in southern Australia are predominantly Mediterranean, and warm or cool temperate. The east coast of Australia including Tasmania, receives reliable rainfall throughout the year. Small pockets of tropical and temperate rainforest exist in northern and southern Australia respectively amongst areas of wet Eucalypt forest.

Seasonal dynamics in vegetation vary significantly in phase and amplitude across Australia, dictated by opposing seasonal rainfall patterns in northern and southern Australia. Seasonal green-up in northern Australia coincides with the onset of the Australian monsoon, beginning in summer (DJF) and extending into autumn (MAM). Seasonal green-up in southern Australia begins in winter (JJA) and extends into spring (SON). Isolated regions in southern Australia exhibit seasonal green-up maxima and minima in summer (DJF) and winter (JJA) respectively. Seasonal dynamics in vegetation are generally dominated by grassy vegetation, as Australian woody vegetation is predominantly evergreen (Donohue et al., 2009).

2.2. Data products used in study

2.2.1. Satellite FAPAR products

The land-surface interacts with PAR through absorption and scattering of incoming PAR. Radiation flux components must be accounted for in a budget framework following the conservation of energy to reconcile incoming PAR with the measured outgoing PAR at the top-of-canopy (Eq. 1). An additional horizontal flux contribution becomes insignificant relative to vertical radiant fluxes at low spatial resolutions typical of satellite remote sensing products (Widlowski, Pinty, Lavergne, Verstraete, & Gobron, 2005). The definition of FAPAR may also vary between products: FAPAR may relate only to direct solar radiation ('instantaneous FAPAR'), diffuse radiation or include both indirect/diffuse radiation. The FAPAR estimate may also relate to a particular instant in time.

This paper considers the inter-comparison of six satellite-derived global FAPAR products. The products are generated from different models, using different optimisation techniques and space-borne measurements from instruments with different specifications (e.g. spectral bands and measurement precisions). The products also correspond to various definitions of FAPAR. Table 1 provides a detailed summary of each FAPAR product.

2.2.1.1. MODIS FAPAR. The MODIS LAI and FAPAR collection 5 products (MOD15A2 and MYD15A2 from Terra and Aqua respectively) are derived from the inversion of a 3D radiative transfer (RT) model that accounts for the heterogeneity (3D structure) of vegetated land-surfaces primarily at the canopy scale (Knyazikhin et al., 1998, 1999; Myneni et al., 2002). Top-of-canopy bidirectional reflectance factors (BRFs) and associated uncertainties from up to seven MODIS spectral bands are used in the inversion and optimisation of the 3D RT model.

A look-up-table is used to identify state-vector solutions (including LAI) consistent with observed top-of-canopy BRFs, from which the mean state-vector is taken as the optimal solution. FAPAR is then estimated from closure of the surface radiation budget. Essential to the MODIS optimisation algorithm are 8 classes of MDC12Q1 global biome classification (Section 2.2.3). The classification makes assumptions on vegetation characteristics (structure/scattering properties/canopy height), degree of heterogeneous cover, soil type and colour and climate. An NDVI-based backup algorithm is applied following the failure to identify an optimal solution. The MODIS FAPAR used here (MOD15A2) is stated as being the FAPAR arising from direct (10:30 h equatorial crossing time) and diffuse radiation (Knyazikhin et al., 1998).

2.2.1.2. MERIS and SeaWiFS FAPAR product. The JRC FAPAR product (Gobron, Pinty, Taberner, et al., 2006; Gobron, Pinty, Aussedat, et al., 2006; Gobron et al., 2008) is derived from a generic vegetation index (Gobron et al., 2000) applicable to any satellite instrument with spectral bands in the near-infrared (NIR), red and blue bands (e.g. Gobron, Pinty, Aussedat, et al., 2006; Gobron, Pinty, Taberner, et al., 2006; Gobron, Pinty, Verstraete, & Govaerts, 1999; Gobron, Pinty, Verstraete, &

Table 1
Technical details of the six satellite-derived FAPAR products.

	MODIS	MERIS	SeaWiFS	MODIS-TIP	VEGETATION	AVHRR
Platform	Terra	EnviSat	OrbView-2(SeaStar)	Terra & Aqua	SPOT VEGETATION (VGT)	NOAA EOS AVHRR
Instrument	MODIS	MERIS	SeaWiFS	MODIS	VEGETATION	AVHRR
Version	5					
Spatial resolution (deg)	0.01°	0.01°	0.01°	0.01°	0.01°	0.01°
Temporal resolution (days)	8	10	10	16	10	30
Time-series (year)	2000–present	2003–2012	1997–2006	200–present	1999–present	1980–2006
Input						
Spectral band (VIS-NIR)	7	3	3	2	3	2
Spectral band uncert.	Y	Y	Y	Y	Y	N
BRFs	Y	Y	Y	N	Y	N
Albedo	N	N	N	Y	N	N
Spectral region	N/A	N/A	N/A	VIS/NIR	N/A	N/A
Radiance type	Top-of-canopy	Top-of-atmosphere	Top-of-atmosphere	Broad-band sfc albedo	Top-of-canopy	Top-of-atmosphere
ATM correction	RT	Blue band	Blue band	RT	RT	N
RT model inversion	Y	Y	Y	Y	Y	N
Type	3D	1D	1D	1D Two-stream	1D	N/A
Optimisation method	Look-up tables	Based on RT models	Based on RT models	Bayesian inversion	Neural network	N/A
Prior information	6-class biome classif.	N	N	A priori PDFs*	N	N/A
Back-up algorithm	NDVI	N	N	N	N	N/A
Rescalling of FAPAR data	N	N	N	N	Y	Y
Cross-instrument calibration	N/A	N/A	N/A	N/A	Y	Y
Calibration (field site) dataset	Y	Y	Y	N	Y	N/A
Post model-fit assessment	N	N	N	Y	N	N
Validation references	Myneni et al., 2002	Gobron, Pinty, Aussedat, et al., 2006; Gobron et al., 2007; Gobron et al., 2008	Gobron, Pinty, Taberner, et al., 2006, Gobron, Pinty, Aussedat, et al., 2006	Pinty et al., 2008; Pinty, Jung, et al., 2011	Baret et al., 2007	Donohue et al., 2008
Output						
FADAR	Yes	Yes	Yes	Yes	Yes	NDVI rescaling
FADAR definition	FADAR from direct (10:30 h) & diffuse radiation	Instantaneous green FAPAR based on direct (10:00 h) radiation	Instantaneous green FAPAR based on direct (12:05 h) radiation	FAPAR/GREEN from diffuse radiation	FAPAR at 10:15 local solar time	Full FAPAR from direct radiation
LAI	Yes	No	No	Yes	Yes	No
Data provider	NASA/Boston University	JRC–EC	JRC–EC	JRC–EC	GeoLand2	CSIRO
2nd provider	AusCover–CSIRO	N/A	N/A	N/A	N/A	AusCover–CSIRO
Data source	ftp://ladstp.nascom.nasa.gov/ www.auscover.org.au	www.fapar.jrc.it	www.fapar.jrc.it	www.fapar.jrc.it	www.geoland2.eu	www.auscover.org.au

Notes: MODIS-TIP Spatial/temporal resolutions of 500 m/8-days are possible. The use of spectral bands in place of broadband albedo is also possible.
* A prior PDFs on all model parameters.

Taberneret, 2002; Meroni et al., 2012). Top-of-atmosphere radiance measurements from MERIS/SeaWiFS are normalised to account for angular variations in illumination and observation geometries. The normalised red and NIR bands are then 'rectified' using the blue band to account for atmospheric scattering. Rectification involves ratios of polynomial functions of the red/blue and NIR/blue bands respectively, the coefficients (*P*) of which are optimised through RT modelling. FAPAR is then computed as a function of the rectified red/NIR bands and the polynomial coefficients *P*.

A 1D (horizontally homogeneous) semi-discrete land-surface-atmosphere coupled RT model (Gobron, Pinty, Verstraete, & Govaerts, 1997; Vermote, Tanré, Deuze, Herman, & Morcette, 1997) was used to model vegetation canopy characteristics and generate a training dataset. The FAPAR represents the instantaneous FAPAR of vegetation under direct illumination (10:00 h equatorial crossing time, Gobron et al., 1999). Accuracy is approximately ±5–10% and agreement with in-situ estimates over different canopy types is ±0.1 (Gobron, Pinty, Taberner, et al., 2006; Gobron et al., 2008).

2.2.1.3. MODIS-TIP. The MODIS-TIP FAPAR/LAI products are generated from the optimisation of a 1D two-stream RT model (JRC-TIP, Pinty et al., 2006) using MODIS VIS/NIR white-sky (bi-hemispherical) albedo (MCD43B3.005) in place of multiple spectral bands (Pinty, Andredakis, et al., 2011). Fundamental land-surface spectral characteristics are maintained by the land-surface albedo while issues related to observation and illumination geometries can be negated as broadband albedo integrates across both angular and spectral domains. Bayesian inversion techniques (Tarantola, 2005) are used to optimise the RT state-vector from the observed albedo constraints. A priori Probability Distribution Functions (PDF) of all seven state-vector parameters (including effective LAI) must be defined and the resulting parameter solutions are a set of a posteriori PDFs. Closure of the surface radiation budget (providing estimates of FAPAR) is achieved after running the JRC-TIP model forward with the set of optimised RT parameters.

Two versions of the MODIS-TIP FAPAR/LAI product are available. The STANDARD and GREEN versions differ in constraints placed on leaf (vegetation canopy) scattering properties (e.g. leaf colour) in the NIR. All models require the specification of leaf scattering properties and may either be (1) assigned to a fixed, generic parameter value (e.g. MERIS/SeaWiFS), (2) parameterised depending on BIOME type (MODIS) or (3) a parameter optimised by the inversion procedure (MODIS-TIP). All products evaluated here, including the MODIS-TIP STANDARD version, use a leaf scattering specification of an average leaf (or standard leaf scenario, see Pinty, Andredakis, et al., 2011 for details). The MODIS-TIP GREEN version uses a different leaf scattering specification (in the form of a different a priori PDF) that is more applicable to a typical green leaf scenario (Pinty, Andredakis, et al., 2011). The STANDARD version is interpreted as the total FAPAR arising from green and non-green vegetation. The GREEN version is interpreted as the FAPAR arising if all vegetation is assumed to be green, as dictated by constraints on the leaf scattering parameter. The different scattering properties result from the more efficient scattering of NIR by green vegetation relative to non-green (yellow/brown) vegetation, thus requiring less effective leaf area (LAI) to generate an equivalent observed signal (Pinty et al., 2009).

2.2.1.4. SPOT-VEG. The Geoland2 Core Mapping Service BioPar provided the SPOT-VEGETATION (SPOT-VEG) GEOV1 FAPAR product (Baret et al., 2013). The product is based on the CYCLOPES FAPAR product (Baret et al., 2007) but has been combined with the MODIS collection 5 FAPAR product (Myneni et al., 2002) and linearly scaled from 0–1 to generate the 'fused' GEOV1 product (Baret et al., 2013; Meroni et al., 2012). Justification for creating a fused product was to limit deficiencies in low/high FAPAR values for MODIS/CYCLOPES respectively, while taking advantage of other qualities of each product, including similarities in FAPAR definition and observation geometry (Baret et al., 2013). The product is thus not completely independent of the MODIS product used in this study. GEOV1 FAPAR corresponds to instantaneous value at 10:15 h local solar time.

The original CYCLOPES FAPAR product was generated using the Scattering by Arbitrarily Inclined Leaves (SAIL) 1D radiative transfer model (Verhoef, 1984) optimised via a neural network (Bacour et al., 2006; Baret et al., 2007). The full time-series consists of observations from two VEGETATION instruments on board SPOT-4 (launched 1998) and SPOT-5 (launched 2002), requiring a preliminary step of instrument cross-calibration. Cloud/cloud-shadow screening, a model-based atmospheric correction and conversion to top-of-canopy Bidirectional Reflectance Factors (TOC BRFs) by accounting for observation and illumination geometries were then applied. The SPOT-VEG retrieval of LAI/fCOVER, including training of the neural network, utilises spectral bands in the red, NIR and SWIR only. The blue spectral band is not used for atmospheric correction due to excessive noise (Baret et al., 2007). Closure of the surface radiation budget is achieved after running the RT model forward with the optimised state parameters, thus providing estimates of FAPAR. Similar to the MERIS FAPAR product, a calibration (or training) dataset has been used and is representative of any land-surface type.

2.2.1.5. AVHRR. AVHRR data have been available since the launch of early National Oceanic and Atmospheric Administration (NOAA) weather satellites. The value of an AVHRR-based product is the long time-series of data, despite limitations arising from broad-spectral bands, out-dated technology and difficulties in cross-instrument calibration. Data extends back to 1981 and allows for long-term temporal trend analyses (e.g. Donohue et al., 2009). The AVHRR product produced for Australia (Donohue et al., 2008) was not generated from an optimised RT model but is instead based on the NDVI.

Cross-instrument calibration, a significant issue across five separate AVHRR instruments, is achieved by considering the 'cover triangle' formed by the red and NIR reflectances in red/NIR spectral space. Important features of this triangle are the soil line and the 'dark point' (see Donohue et al., 2008 for details). Successful cross-instrument calibration results from the adjustment of red/NIR AVHRR radiances from each sensor such that the cover triangle is invariant in time. Anchoring the soil line and dark point requires both bright and dark geographic targets (salt lakes and water bodies respectively) that have a time invariant albedo. FAPAR estimates were then calculated by rescaling the NDVI values to 0–0.95 (Donohue et al., 2008).

2.2.2. Vegetation fractional cover

Two datasets, consisting of in-situ and satellite-derived estimates of vegetation fractional cover, are used in this study. Both datasets consist of the fractional cover of three classes: photosynthetically active material (PV), non-photosynthetically active material (NPV) and bare soil (BS). Both datasets conform to the definition of fraction cover (of PV/NPV/BS) as that over the background from a nadir viewpoint.

2.2.2.1. In-situ estimates. An extensive database of ~800 in-situ vegetation fractional cover (FC) estimates across Australia was compared with satellite-derived FAPAR estimates. The in-situ dataset (hereinafter referred to as the FC-dataset) contains FC field measurements (Muir et al., 2011) obtained from the following field campaign programme and datasets: (1) State-Wide Land Cover And Trees Study (SLATS) from the Department of Environment and Resource Management, Queensland; and (2) the Australian ground cover reference sites database from the Australian Bureau of Agricultural and Resource Economics and Sciences.

The FC-dataset (Fig. 1A) consists of in-situ estimates of PV, NPV and BS at three defined vegetation levels: ground cover (PV/NPV/BS fractions that sum to 1), mid-story vegetation (PV/NPV fractions at <2 m) and over-story vegetation (PV/NPV fractions at >2 m). Typical field-site dimensions are 100 m × 100 m (~1 ha). Where possible, sites

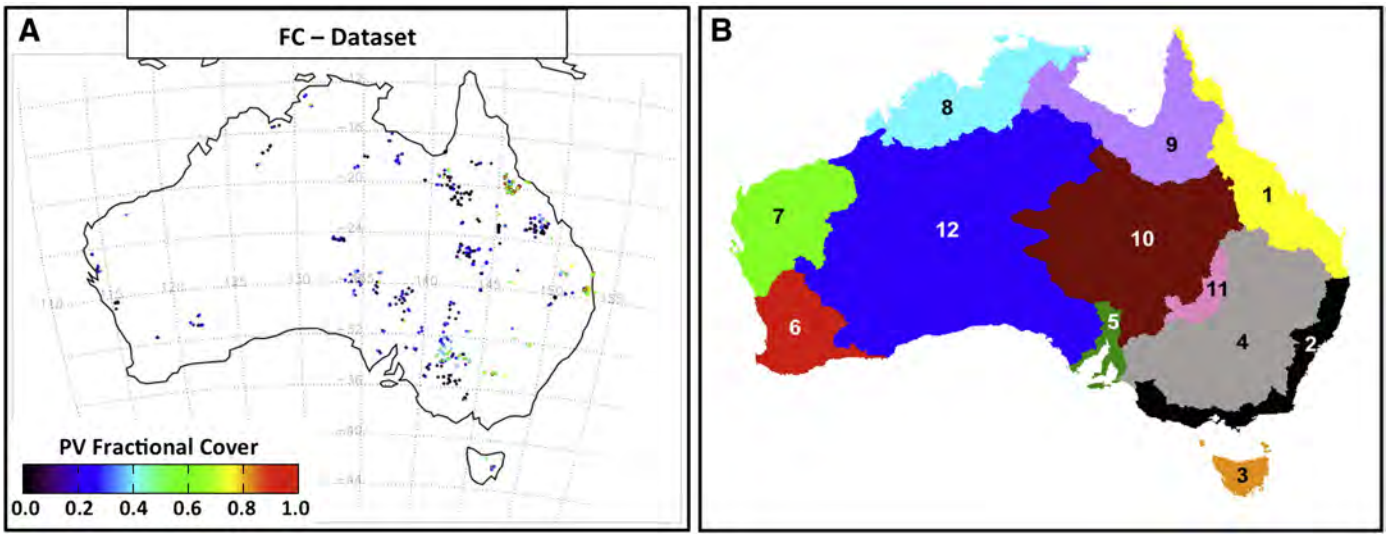

Fig. 1. A: Spatial coverage of in-situ estimated vegetation fractional cover (FC-dataset). Colour scale indicates PV fractional cover. B: Drainage divisions across Australia. NE Queensland (1), SE Australian coast (2), Tasmania (3), MDB (4), Western Australia Coast (6, 7), Northern Australia (8, 9), Central Australia (5, 10, 11) and the Western Plateau (12).

were chosen to be representative of the vegetation cover at larger spatial scales typical of satellite products. Appendix A describes the sampling strategy applied (Muir et al., 2011) and the calculation of the total exposed PV/NPV/BS fractional cover apparent from above the canopy (hereinafter referred to as PV-FC, NPV-FC and BS-FC respectively).

2.2.2.2. Satellite-derived estimates. A satellite-derived MODIS vegetation fractional cover product for Australia (hereinafter referred to as the SD-FC product) (Guerschman et al., 2009) consists of the fractional cover of three end-member classes: photosynthetic-active material (PV), non-photosynthetic active material (NPV) and bare soil (BS). These end-members are derived from two spectral indices: the NDVI and the ratio of MODIS bands 7 (~2100 nm) and 6 (~1650 nm) that is sensitive to spectral characteristics of dry/woody vegetation matter in the short-wave infrared (SWIR) spectral region. The product was validated using both field data and Hyperion hyperspectral satellite data over northern Australia (Guerschman et al., 2009) and ongoing field campaign programmes.

2.2.3. Region classifications across Australia

Three geographic classifications are used in this study. One classification is based on drainage divisions (Fig. 1B), with each division consisting of an amalgamation of individual drainage basins (NLWRA, 2000, 2001). A set of eight drainage divisions is used in this study:

North-East Queensland Coast	Western Australian Coast
South-East Australian Coast (NSW/VIC)	Northern Australia
Tasmania	Central Australia
Murray–Darling Basin (MDB)	Western Plateau

The second geographic classification, the National Vegetation Information System (NVIS), is based on vegetation type (NVIS, 2007). The classification consists of 27 vegetation groups (e.g. tropical and temperate rainforest, Eucalyptus forests, woodlands, shrublands, savanna and grasslands, and cleared agricultural land). The third geographic classification is the MODIS global biome classification (MDC12Q1, updated annually). Eight biomes from this classification are used in the MODIS LAI/FAPAR product retrieval:

Broadleaf evergreen trees	Shrublands
Broadleaf deciduous trees	Savanna
Needle-leaf evergreen trees	Grasslands & cereal crops
Needle-leaf deciduous trees	Broadleaf crops

2.3. Evaluation of the global FAPAR products: methodology

The methodology devised to evaluate the six global FAPAR products over Australia consists of two approaches: 2.3.1. An evaluation based on direct comparisons within different geographic regions across Australia; and 2.3.2. An evaluation using in-situ and satellite-derived estimates of vegetation fractional cover, categorised by vegetation type/biome.

2.3.1. Evaluation based on direct comparisons between products

The FAPAR time-series from each product was partitioned into a seasonal and a base-level component, hereinafter referred to as recurrent and persistent FAPAR. The components are associated with recurrent (grassy) and persistent (woody) vegetation biomes (Donohue et al., 2009) and the partition algorithm (Appendix B) follows Donohue et al. (2009), Lu, Raupach, McVicar, and Barrett (2003) and Roderick, Noble, and Cridland (1999). Seasonal variation and long-term, base-level changes in FAPAR were then evaluated separately by directly comparing all products within each drainage division (Section 2.2.3) across Australia.

2.3.2. Evaluation based on comparisons to vegetation fractional cover

FAPAR product evaluation using a physically consistent independent estimate is not possible in Australia due to a lack of in-situ FAPAR measurements. An extensive database of in-situ estimated vegetation fractional cover can instead be used, augmented by a similarly defined satellite-derived product.

Healthy, green and photosynthetically active vegetation exhibits very little scattering of PAR (i.e. green vegetation is close to a 'black-leaf limit'). Incoming PAR is instead absorbed by the vegetation or passes through gaps in vegetation cover unhindered. Therefore, one can write (Pinty et al., 2009):

$$A_{veg}(u_0, \lambda_{VIS}) \approx 1 - T_{Veg}^{Uncoll}(u_0) \quad (2)$$

$$A_{veg}(u_0, \lambda_{vis}) \approx 1 - e^{-k\frac{LAI(u_0)}{u_0}} \quad (3)$$

In addition, Gobron, Pinty, Taberner, et al. (2006) showed that:

$$A_{veg}(u_0, \lambda_{VIS}) \approx FIPAR(u_0) \quad (4)$$

with a typical error of ~0.1, where FIPAR is the Fraction of Intercepted PAR. Eq. (2) suggests that the theoretical relationship between FAPAR

and FC is ~1:1. Radiative transfer simulations using the CanSPART two-stream radiative transfer scheme (Haverd et al., 2012; Lovell, Haverd, Jupp, & Newnham, 2012) reveal a sensitivity range between FAPAR and FC of 0.96–1.17, a result consistent with that provided by Pinty, Clerici, et al. (2011)). Details of the CanSPART simulations are given in Appendix C. Based on the CanSPART simulations and previous literature, we assume that:

$$A_{veg}(u_0, \lambda_{VIS}) \approx FIPAR(u_0) \approx FCover(u_0) \quad (5)$$

Note:

$A_{veg}(u_0,\lambda_{VIS})$	The fraction of absorbed PAR (FAPAR)
T_{Veg}^{Uncoll}	The fraction of PAR transmitted through the canopy that has not collided (interacted) with vegetation
u_0	Cosine of the sun zenith angle
LAI	Effective LAI
k	0.5
$FIPAR(u_0)$	Fraction of intercepted PAR
$FCover(u_0)$	Fraction of vegetation cover

One can estimate FAPAR from vegetation FC and calculate the resulting effective LAI via a commonly used Beer–Bouger–Lambert's relationship (Eq. 3). This 1:1 relationship provides a basis for evaluating FAPAR estimates using in-situ FC estimates (specifically PV-FC).

To compare against the in-situ field estimates of PV-FC, the satellite 3D data cubes were sampled at their respective native spatial resolution. Extracted FAPAR estimates were obtained at the same location in space and time to in-situ FC estimates, employing linear interpolation between adjacent satellite grids where appropriate. Certain products provide a single time-stamp for each satellite grid whereas others provide a time period for which the satellite grid is considered representative. Spatial sampling involved extracting FAPAR estimates from the pixel closest to the field site location as well as an average FAPAR estimate from a 3 × 3 pixel-matrix overlying the field site. The FC field sites were also stratified using the NVIS vegetation group classification and 8 classes of the MODIS biome classification.

To compare against the satellite-derived estimates of PV-FC, the satellite 3D data cubes were resampled to the resolution of the SD-FC product. Regions of homogeneous fractional cover (R_{HFC}) of PV, NPV and BS (fractional cover >80%) were identified at each time-step (t_f) from the fractional cover product time-series. The corresponding mean FAPAR estimate from each FAPAR product within each R_{HFC} was then extracted at the time-step closest to t_f. A FAPAR time-series for regions of homogeneous cover of PV, NPV and BS was thus generated for each product.

3. Results

3.1. Evaluation based on direct comparisons between products

3.1.1. Comparison of mean FAPAR estimates

Fig. 2A presents the overall mean FAPAR climatology (MFC). The annual FAPAR climatology of each satellite product, calculated over the entire time-series of each product respectively, was used to generate the MFC. Annual climatologies calculated over a common time-period (2003–2006) generated a similar MFC (not shown) to that provided in Fig. 2A. Continental-scale spatial gradients in FAPAR mirror annual rainfall gradients across Australia (Fig. 2B), with a divergence occurring in Northern Australia due to factors limiting productivity during certain times of the year. Correlated spatial gradients in FAPAR and precipitation, evident in Fig. 2A and quantified within different drainage basins (Section 2.2.3, Fig. 1B) in Table 2, are consistent with water limitation impacting productivity across much of mainland Australia.

Fig. 3 presents the difference between each FAPAR annual climatology and the MFC. Using the MFC as a reference, the degree to which any single product differs from other products is clearly related to the density of vegetation cover. The degree to which products differ from the MFC is therefore both spatially heterogeneous and associated with FAPAR spatial gradients.

3.1.2. FAPAR persistent component comparison

Fig. 4 presents the time-series of the persistent FAPAR component from each product within different Australian drainage divisions. Averaging across Australia (1), the spread across the products is uniform with no apparent outlier. In highly vegetated coastal regions (e.g. NE Queensland (2), SE Australia coast (3)), MERIS and SeaWiFS generate relatively low FAPAR estimates. A similar result (not shown) occurs in NVIS-classified forested regions across Australia and at forested flux tower sites such as Tumbarumba (Leuning, Cleugh, Zegelin, & Hughes, 2005) and Wallaby Creek (Kilinc, Beringer, Hutley, Haverd, & Tapper, 2012) (see ozflux.org.au). In Tasmania (4), there is a particularly large spread across the products. Overall, the degree of clustering amongst the different products changes across the continent.

Temporal features consistent across all products are nonetheless evident in Fig. 4. A clear positive FAPAR anomaly from late 2010 through to 2012 is present in most regions, associated with anomalously high annual rainfall and hydrological recharge across much of the continent (National Climate Centre, 2012, Boening, Willis, Landerer, Nerem, & Fasullo, 2012; Fasullo, Boening, Landerer, & Nerem, 2013). The effects of severe drought conditions persisting across eastern Australia during the 2000s are also evident, particularly in the Murray–Darling Basin (5). Anomalously low FAPAR estimates occur in 2003, 2007 and 2009. For products extending back into the 1990s, the 2000s are identified as having persistently low FAPAR due to prolonged periods of below-average rainfall in the Murray–Darling Basin (Daniell, 2009; McGrath et al., 2012; Murphy & Timbal, 2008; Ummenhofer et al., 2009).

3.1.3. FAPAR recurrent (seasonal) component comparison

Fig. 5 presents the seasonal climatology (recurrent FAPAR component, smoothed using a 1-month moving average) for all products in each drainage division. While all products show agreement in seasonal phase (excluding Tasmania, 4), seasonal magnitudes in most regions are clearly different. SPOT-VEG and AVHRR routinely show greater seasonal magnitudes whereas MODIS, MERIS, SeaWiFS and MODIS-TIP show reduced magnitudes. The shape in seasonality as well as the timing in seasonal maximums/minimums also varies. In northern Australia (7) where the summer monsoon (Dec–Apr) dictates seasonal green-up in tropical dry savannas and woodlands, timing in the seasonal maximum varies by ~30 days amongst the products. Rates of senescence following the seasonal maximum also vary.

The seasonal winter/spring green-up (Jun–Nov) along the SE coast of Australia (3) is particularly inconsistent, with some products indicating a broad seasonal maximum whereas others show a relatively short seasonal maximum. Note the disagreement between MERIS and SeaWiFS, overall found to be in high agreement. Seasonal variation in Tasmania (4) is also inconsistent, where different regions within Tasmania have opposing seasonal modes: maxima/minima in summer/winter and maxima/minima in winter–spring/summer (typical of SE Australia).

3.2. Evaluation based on comparisons to vegetation fractional cover

3.2.1. Comparison with in-situ field measurements of PV, NPV and BS

Fig. 6A plots satellite-derived FAPAR against in-situ estimated vegetation fractional cover (specifically PV-FC, see Section 2.2.2). The plotted FAPAR estimates were obtained from the closest single pixel to the reported field-site location. Little discernable difference was observed when plotting the average FAPAR estimate from a 3 × 3 pixel-matrix overlying the field site. Table 3 provides summary statistics of the linear regression between PV-FC and FAPAR (corresponding to the dashed line-of-best-fit in Fig. 6A). No product produces a ~1:1 relationship between FAPAR and PV-FC and all products show different sensitivities of FAPAR to PV-FC (coefficient of linear regression in Table 3). Note the

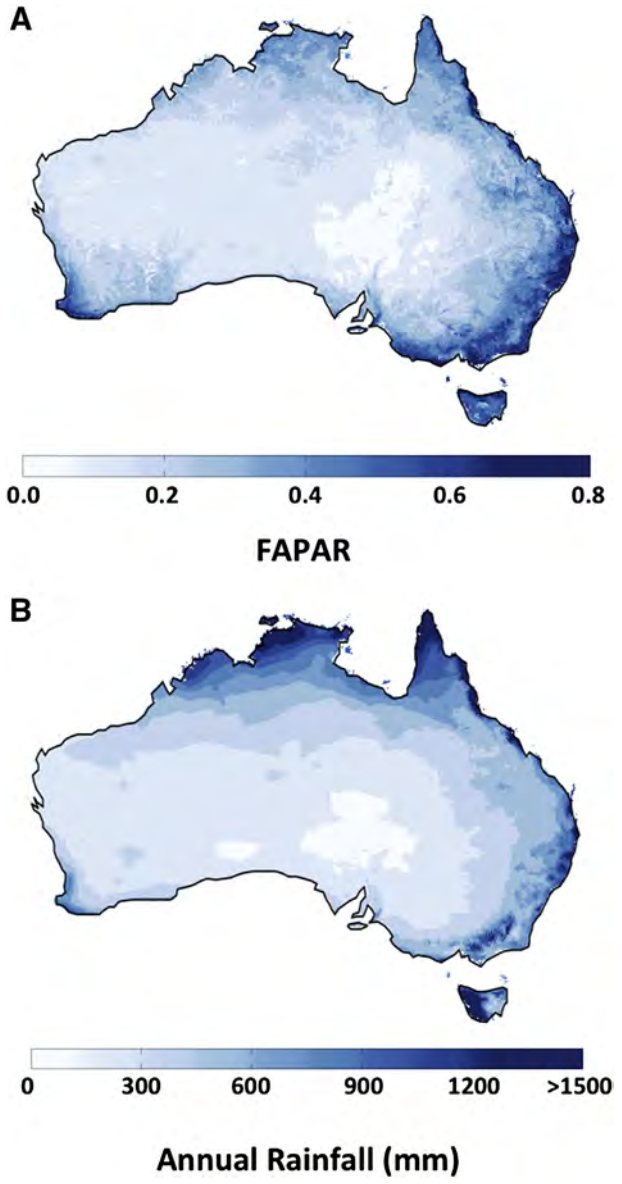

Fig. 2. A: MFC — annual mean FAPAR climatology. B: Mean annual precipitation (mm).

difference in sensitivities between the two versions of the MODIS-TIP product (Table 3), related to the standard-leaf/green-leaf scenarios. All products show differing levels of scatter around the line-of-best-fit (Lin. Reg. SD in Table 3,). Some products (MODIS, MODIS-TIP, AVHRR) show a positive offset in FAPAR within regions of little or no PV fraction (Intercept in Table 3). Other products (MERIS/SeaWiFS/SPOT-VEG) appear on average to correctly identify regions of very low PV-FC within specified uncertainty tolerances of ~0.1 (Gobron, Pinty, Taberner, et al., 2006; Gobron et al., 2008).

Fig. 6A indicates the fraction of over-story (green) vegetation (>2 m) contributing to PV-FC. High proportion of over-story vegetation cover represents field sites in forested biomes while the remaining sites lie in regions of significant ground cover (e.g. grassland, savannah, shrubland and agricultural biomes). This stratification clearly identifies two groups of field sites with similar estimates of PV-FC but considerably different FAPAR estimates from MODIS and SPOT-VEG. Excluding field sites with over-story fractional cover >0 results in a similar fit to the in-situ data across all products and no remaining site differentiation (Table 4). SPOT-VEG retains a somewhat higher sensitivity in FAPAR with increases in PV-FC.

Table 2
Spatial correlation between the mean FAPAR climatology (MFC) and precipitation climatology (Fig. 2) for each drainage division listed in Section 2.2.3 and Fig. 1B.

Drainage division	Spatial correlation
North-East Queensland Coast	0.72
South-East Australian Coast (NSW/Vic)	0.66
Tasmania	−0.08
Murray–Darling Basin (MDB)	0.82
Western Australian Coast	0.82
Northern Australia	0.78
Central Australia	0.75
Western Plateau	0.43
Australia	0.73

Fig. 6B repeats the scatter plots of Fig. 6A but indicates the MODIS land-cover biome classification (MDC12Q1) for each field site (see Section 2.2.3). Similar to Fig. 6A, field sites classified as primarily broad-leaf evergreen generate considerably higher MODIS FAPAR estimates relative to other biomes with the same level of PV-FC. Most field sites with a significant level of over-story PV fractional cover (Fig. 6A) are correctly classified as forest. This suggests that, with the available MDC12Q1 biome classes, land-cover miss-classification across the field sites is not a significant problem.

3.2.2. Comparison to the satellite-derived fractional cover product

Fig. 7A presents the FAPAR time-series for the 6 products in regions of predominantly PV, NPV and BS. Table 3 provides statistics related to the time-series presented in Fig. 7A. Fig. 7B presents the number of grids where the fractional coverage from the SD-FC product is >80% for PV, NPV and BS. Homogeneous cover in PV and BS frequently occur in coastal regions and central Australia respectively. Areas of homogeneous NPV occur infrequently in relatively small, contiguous regions.

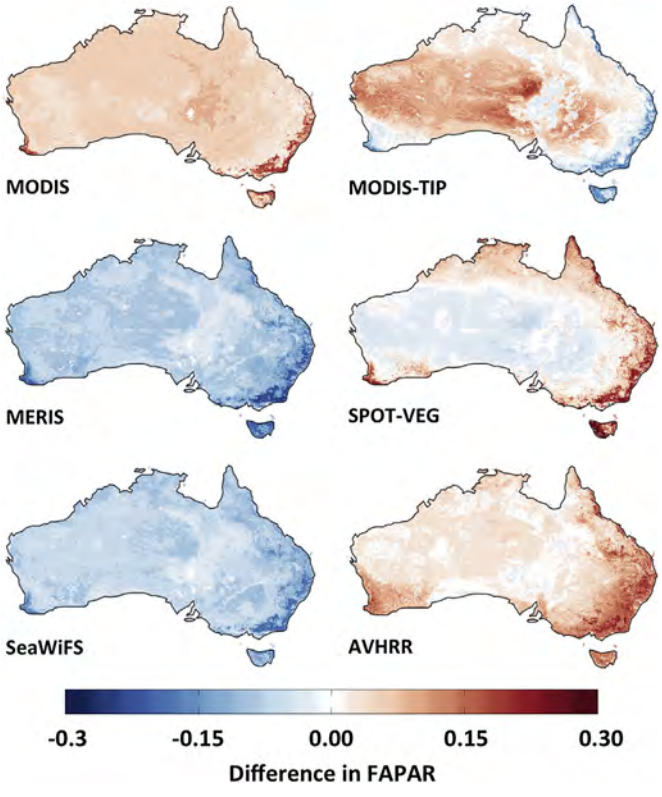

Fig. 3. Difference maps between the individual annual FAPAR climatology for each product and the mean FAPAR climatology (MFC, Fig. 2A) across all products.

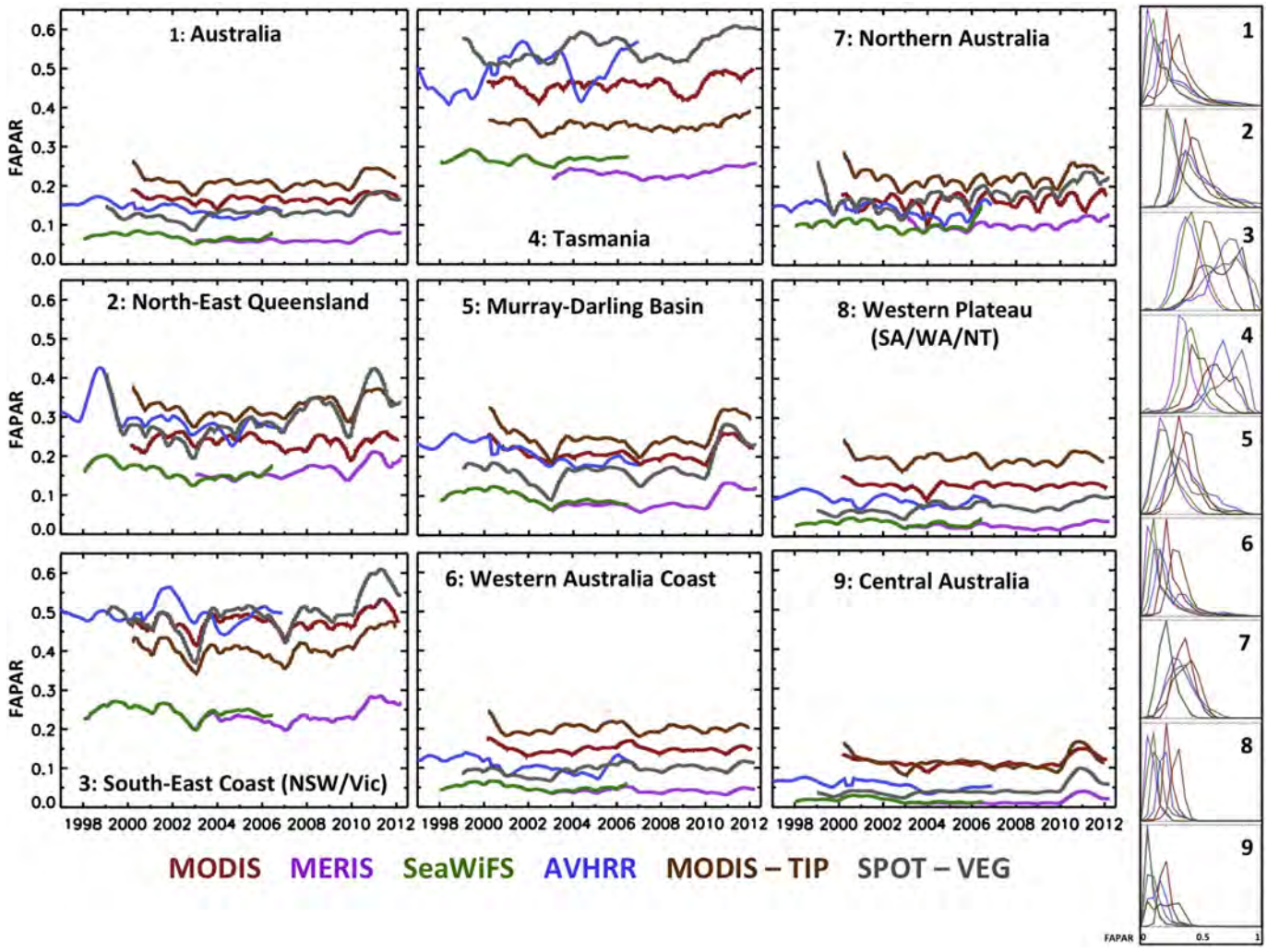

Fig. 4. Time-series of the different FAPAR satellite products (persistent vegetation component) for Australia and 8 Australian drainage divisions. The plots on the right present the frequency histograms of each product (full FAPAR signal) for each region.

Immediately apparent from Fig. 7A are different base-level FAPAR estimates in regions of little or no green vegetation cover (NPV and BS time-series). MERIS, SeaWiFS and SPOT-VEG generate FAPAR estimates of <0.05 whereas MODIS, MODIS-TIP and AVHRR show a significant positive offset (Table 3). These offsets are consistent with those apparent from comparisons to in-situ PV-FC estimates (Fig. 6, Table 3) and largely explain why products differ in the semi-arid regions of central Australia.

After accounting for offsets in base-level FAPAR, mean FAPAR estimates in regions of predominantly PV fractional coverage (green vegetation) also differ (range in FAPAR in Table 3). SPOT-VEG generates the highest FAPAR. MERIS/SeaWiFS/MODIS-TIP generate low FAPAR, consistent with systematically low FAPAR in regions of dense vegetation coverage (e.g. SE coast of Australia, Fig. 4).

The differences in FAPAR sensitivity to PV-FC identified in Fig. 7A are consistent with the differences in sensitivity identified from comparisons to in-situ field data (Fig. 6, Table 3). The close association between in-situ estimated sensitivity and biome type likely extends to a larger spatial scale provided by the SD-FC product, with biome type influencing the range in FAPAR of certain products across Australia (Table 3). MODIS forest biomes (Fig. 6B) occur predominantly in regions of high PV-FC (Fig. 7B). The range in SPOT-VEG FAPAR may also be a result of global rescaling to 0–1 (Baret et al., 2013; Meroni et al., 2012). The range in FAPAR of the MODIS-TIP GREEN version (Table 3) was found to be less than that of the STANDARD version. Thus, in addition to biome type, assumptions related to vegetation scattering properties influence the range in FAPAR across the continent.

A comparison between different backgrounds (BS and NPV) can be made from Fig. 7B and Table 3, where a positive offset in FAPAR between a NPV background relative to a BS background may suggest a positive contribution from NPV material to a FAPAR signal. However, most products exhibit an insignificant difference between the two backgrounds. MODIS-TIP exhibits an unexpected large positive difference between BS background relative to NPV background. This interesting discrepancy should be treated with caution as it predominantly occurs in small, contiguous regions of savanna in northern Australia (Fig. 7B) and is not apparent in comparisons with in-situ data (not shown).

4. Discussion

Despite ostensibly significant disagreements, the FAPAR satellite products do show robust spatial and temporal patterns across Australia. Moreover, the disagreements can be partially attributed to a consistent offset in FAPAR in some products across much of the continent. An offset may be accounted for in certain applications through product-specific model retuning. This likely explains why different FAPAR products used in biospheric diagnostic models (Haverd et al., 2013; Seixas et al., 2009) generate highly consistent continental mean NPP/NEP estimates but reduced consistency in regional estimates and seasonal variation. The comparison of the FAPAR products to the SD-

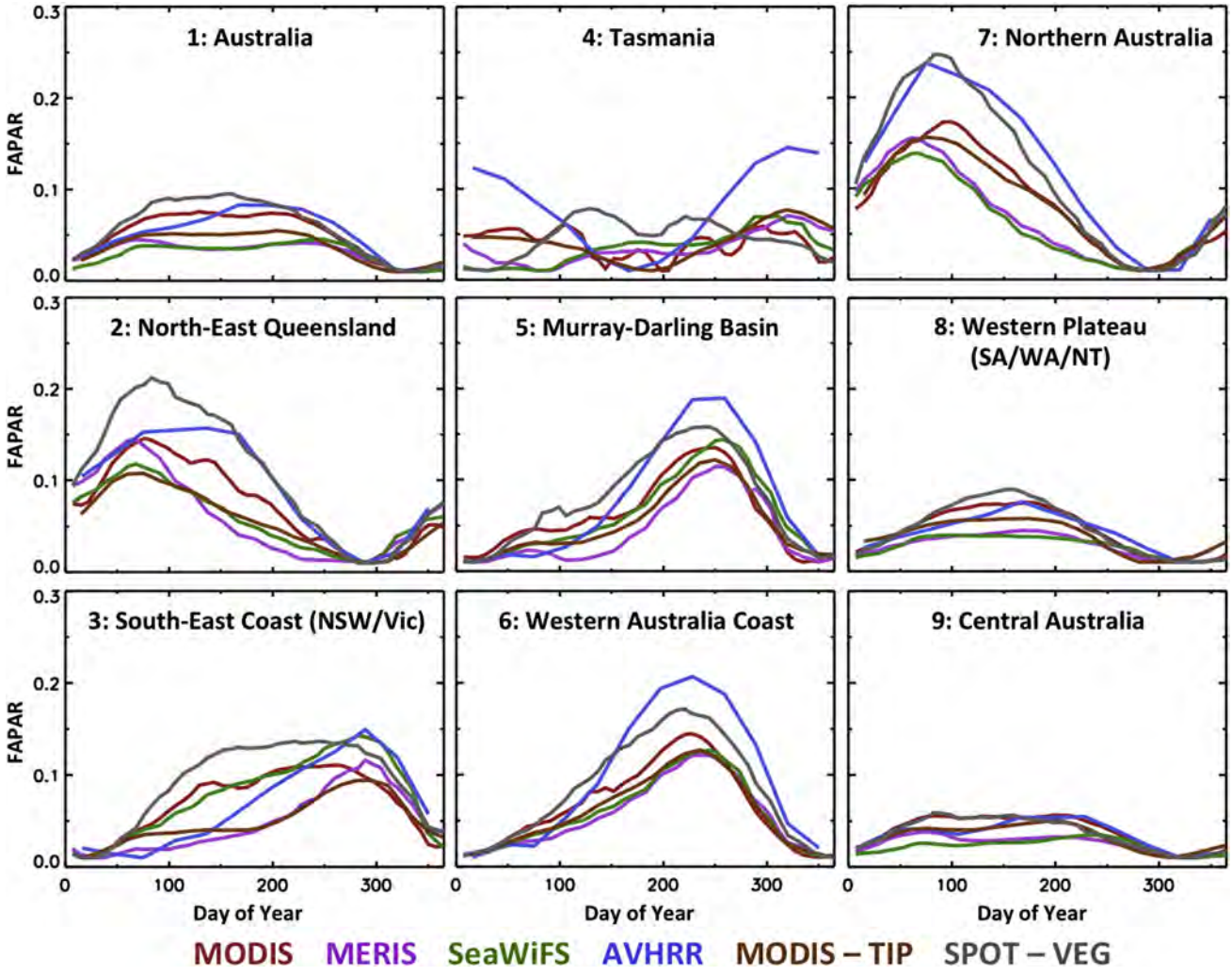

Fig. 5. Seasonal climatology plots of the different FAPAR satellite products (recurrent vegetation component) for Australia and 8 Australian drainage divisions. Note: All seasonal plots have been adjusted to a common seasonal minimum FAPAR value of 0.01. This aids in comparing the amplitude and timing of the seasonal maximums/minimums and rates of green-up and senescence. A 1-month moving average smoothing filter has been applied to all seasonal climatologies except AVHRR.

FC product is generally consistent with the comparison to the in-situ field estimates of vegetation fractional cover.

Physically consistent in-situ field estimates have been used to validate the FAPAR products (Table 5). Fensholt, Sandholt, and Rasmussen (2004) and Huemmrich, Privette, Mukelabai, Myneni, and Knyazikhin (2005) identified a positive bias of ~0.2 in MODIS FAPAR estimates, consistent with this study. Gobron, Pinty, Aussedat, et al. (2006), Gobron et al. (2008) estimated the MERIS and SeaWiFS FAPAR uncertainty as ~0.1, consistent with the small offsets identified here. As these uncertainty estimates are based on relatively few field sites, their applicability at larger spatial scales and/or within different geographical regions and biomes may be limited. In addition, the theoretical (or simulated) uncertainty in LAI (and consequently FAPAR) derived from remotely-sensed observations varies non-linearly with LAI (FAPAR) (Myneni et al., 2002; Pinty, Clerici, et al., 2011) and applies to all products. A reduction in sensitivity of a remotely-sensed signal to increasing LAI up to a point of signal saturation (no sensitivity, Shabanov et al. 2005) leads to a loss of observational constraint and an increase in parameter uncertainty. The point of signal saturation varies depending on the product as well as in space and time (Myneni et al., 2002) but typically occurs at an LAI of 3–4 (Pinty, Andredakis, et al., 2011; Pinty, Jung, et al., 2011) for MODIS-TIP and an LAI of ~3.5 for MODIS (Shabanov et al. 2005).

Fig. 8 provides an analysis of the a posteriori uncertainty ($1.\sigma$) in the MODIS-TIP FAPAR. Minimum FAPAR uncertainty estimates are 0.4–0.5 and correspond to the MODIS-TIP base-level FAPAR estimates described previously. As FAPAR (LAI) increases, uncertainty in FAPAR (LAI) increases as expected (up to ~0.8 uncertainty in FAPAR). More surprising is an increase in FAPAR for very low values of FAPAR (<0.3), a result related to uncertainties in soil background (Pinty, Clerici, et al., 2011). The positive offset in base-level MODIS-TIP FAPAR mentioned previously (Figs. 6 and 7B) is consistent with the estimated uncertainty in FAPAR. The Bayesian inversion methodology of MODIS-TIP allows for the propagation of a priori uncertainties (e.g. error in observations) through to the state parameters (LAI, FAPAR), providing a theoretical uncertainty across the full range of LAI/FAPAR.

The comparison of satellite-derived FAPAR to in-situ estimates of PV-FC reveals a relationship as <1:1 for all products concerned (coefficient of linear regression range: 0.30–0.57, Table 3). This is in contrast to the expected ~1:1 theoretical sensitivity as shown previously in Section 2.3.2. The linear 1:1 relationship between FAPAR/FIPAR and vegetation FC is appropriate when FAPAR is measured directly. However, remotely sensed FAPAR is obtained indirectly through closure of the surface radiation budget, constrained by observed scattering of NIR radiation rather than observed absorption of PAR. Perturbing effects of the background albedo within the visible (VIS) spectrum (corresponding to PAR) prevent observed changes in VIS albedo (or red BRFs) to estimate FAPAR directly. The linear relationship between changes in VIS and NIR albedo defines a so-called 'soil-line' (Chi, 2003) to account for changes in background NIR albedo. NIR scattering (illustrated by

positive departures from the soil-line in VIS/NIR space) is used in remote-sensing RT algorithms to constrain estimates of effective (domain-averaged) LAI, from which FAPAR is estimated via closure of the surface radiation budget (Eqs. 1, 3). Departures from the soil-line due to NIR scattering also form the basis of vegetation indices such as the NDVI, variations of which are correlated with those of FAPAR (Fensholt et al., 2004; Liang et al., 2012; Myneni & Williams, 1994).

The degree of NIR scattering by vegetation (soil) is dependent on leaf (soil) scattering properties (e.g. leaf/soil colour). Vegetation scattering properties vary depending on vegetation species (Pinty et al., 2009), biome type, green-leaf/standard-leaf scenarios and even leaf maturity (young vs. mature leaves, Pinty, Jung, et al., 2011). The differences in the regression slopes between the two versions of the MODIS-TIP FAPAR product (Table 3) are attributed to differences in constraints on NIR vegetation scattering properties (Pinty, Clerici, et al., 2011). Both leaf and soil scattering properties are assigned to each MODIS biome type (Shabanov et al. 2005; Myneni, Nemani, & Running, 1997). Assumed leaf scattering properties, necessary within RT retrieval algorithms and averaged over a relatively large spatial domain, will impact the estimated effective LAI and resulting FAPAR estimates. Consequently, the relationship between FAPAR and FCover (such as PV-FC) will be impacted. Departures from the correlated variation in NIR/VIS background (represented by the soil-line) and a lack of consistency in observation/illumination geometries between remotely sensed observables (e.g. FAPAR resulting from direct and/or diffuse radiation) and in-situ field measurements of FCover will also impact the FAPAR/FCover relationship. Finally, the observed signal due to NIR scattering is impacted by physiological changes in vegetation (such as stress resulting from water/nutrient constraints or leaf maturity) impacting leaf optical properties (Huemmrich et al., 2005). Such changes in the observed NIR signal will impact the retrieved LAI (and FAPAR) estimates but may not be apparent when making in-situ estimates of vegetation fractional cover that, in the case of the PV-FC estimates, only reflect the presence of living vegetation. A 1:1 relationship instead acts as an upper limit:

$$FAPAR \leq FIPAR/FCover$$

and is valid only under circumstances when numerous model

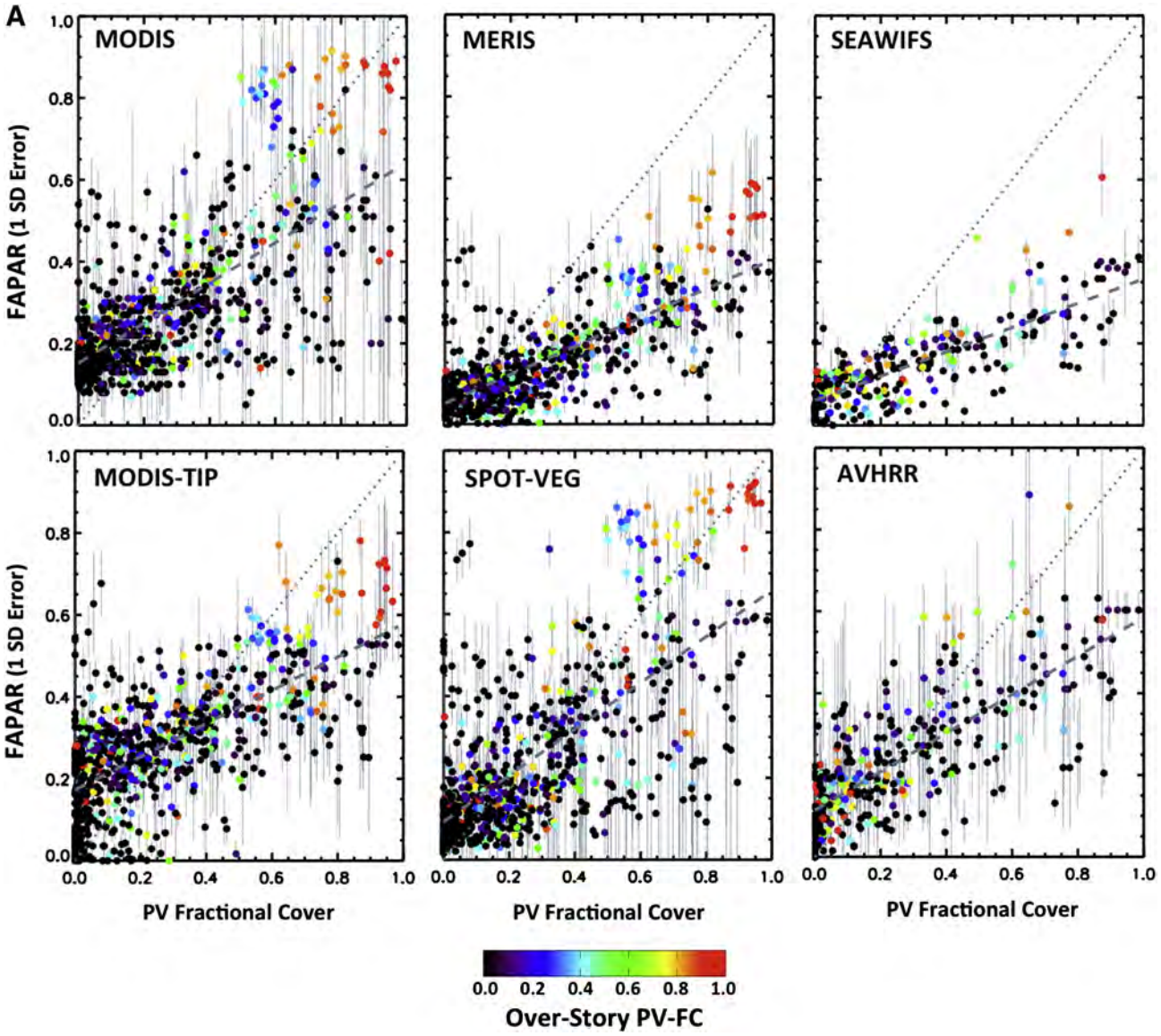

Fig. 6. A: Scatter plots of each FAPAR product with field estimates of PV fractional cover. Colour bar represents the proportion of over-story PV fractional cover contributing to the total exposed PV fractional cover (PV-FC) from all three vegetation levels. Error bars represent both spatial and temporal variability of the satellite FAPAR mean estimate. Solid grey line represents a 1:1 relationship and dashed grey line represents the line of best fit through the data. B: Scatter plots of each FAPAR product with field estimates of PV fractional cover as in Fig. 6A. Also indicated is the MODIS land-cover classification (MCD12Q1) identified for each field site.

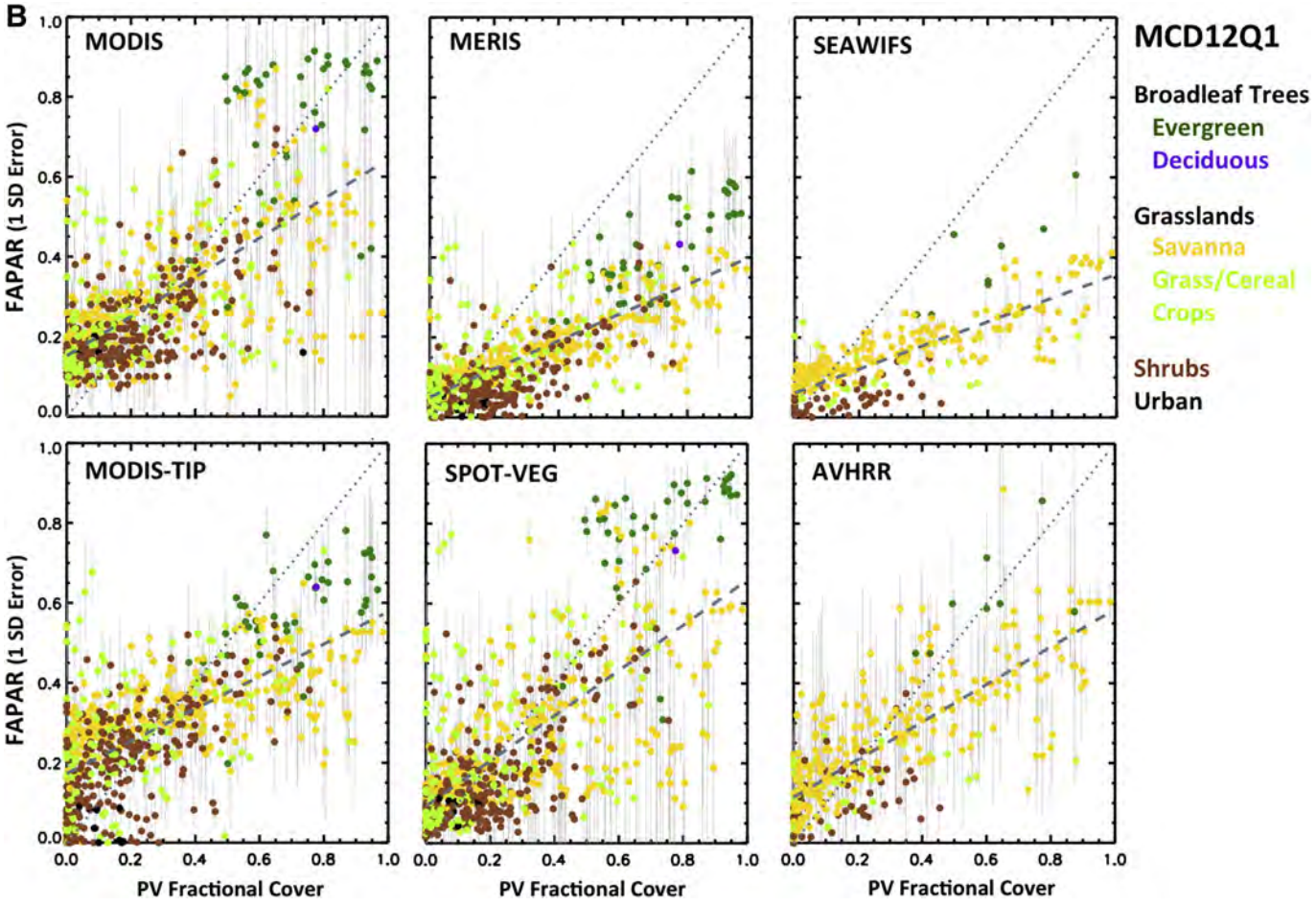

Fig. 6 (*continued*).

assumptions, such as those related to vegetation/soil scattering properties and consistency in observation/illumination geometries, are satisfied.

A number of factors thus influence the relationship between FAPAR and FCover (Fig. 6), the range in FAPAR observed across the continent (Section 3.2.2, Fig. 7A, Table 3) and ultimately the degree of agreement

Table 3
Statistics from the regression analysis (line-of-best-fit) presented in Fig. 6A. Statistics from the comparison to the SD-FC dataset presented in Fig. 7A.

	In-situ FC dataset						SD-FC dataset							
							Mean FAPAR						Range	
Model	No. obs	R^2	SS-resid	X-Y correl.	Lin-coeff.	Intercept	PV		NPV		BS		PV-BS	
MODIS	820	0.47	0.13	0.69	0.49	0.15	0.73	(0.15)	0.18	(0.08)	0.15	(0.03)	0.58	(0.15)
MERIS	771	0.58	0.08	0.76	0.35	0.05	0.44	(0.14)	0.07	(0.05)	0.02	(0.02)	0.42	(0.14)
SeaWiFS	297	0.64	0.06	0.80	0.30	0.06	0.47	(0.13)	0.08	(0.06)	0.03	(0.02)	0.44	(0.13)
MODIS-TIP (STD)	770	0.46	0.11	0.68	0.40	0.17	0.58	(0.13)	0.06	(0.07)	0.28	(0.05)	0.30	(0.14)
MODIS-TIP (GRE)	770	0.45	0.09	0.67	0.31	0.15	0.48	(0.10)	0.05	(0.06)	0.25	(0.05)	0.23	(0.11)
SPOT-VEG	791	0.48	0.15	0.69	0.57	0.09	0.80	(0.08)	0.13	(0.09)	0.06	(0.03)	0.74	(0.09)
AVHRR	355	0.59	0.10	0.77	0.47	0.11	0.78	(0.12)	0.15	(0.14)	0.13	(0.05)	0.65	(0.13)

Key

In-situ FC dataset	
No. obs.	Number of observations
Lin-coeff	Coefficient of linear regression between FAPAR and PV-FC
Intercept	y-intercept of linear regression
R^2	R^2 statistic
SS-resid	Linear regression standard deviation (residual sum of squares) Interpreted as the scatter around the line of best fit, not the standard error of the lin-coeff
X-Y correl.	Correlation between FAPAR and PV-FC
SD-FC dataset	
Mean FAPAR	Mean FAPAR estimate in regions of predominantly (>80% fractional cover) PV, NPV or BS calculated from the time-series presented in Fig. 7A Values in brackets are the estimated standard deviation in FAPAR

Table 4
Statistics from the regression analysis (line-of-best-fit) as in Table 3 but with the exclusion of field sites classified as broadleaf evergreen/deciduous (MDC12Q1) in Fig. 6B.

MODEL	No. obs	R^2	SS-resid	X-Y correl.	Lin-coeff.	Intercept
MODIS	763	0.36	0.10	0.60	0.34	0.17
MERIS	718	0.46	0.07	0.68	0.27	0.06
SeaWiFS	233	0.64	0.05	0.80	0.27	0.06
MODIS-TIP (STD)	713	0.33	0.11	0.57	0.33	0.18
MODIS-TIP (GRE)	713	0.33	0.09	0.57	0.26	0.16
SPOT-VEG	736	0.35	0.12	0.59	0.40	0.11
AVHRR	346	0.59	0.10	0.77	0.44	0.12

between products. An additional factor identified in this study is biome type. Increased agreement was observed at sites classified as savanna/grassland, shrubland and managed lands (including agricultural/cropping land). Substantial disagreement occurs instead at sites classified as forest. MODIS exhibits a near twofold increase in FAPAR at forest sites (consistent with sites containing a high fraction of over-story vegetation cover) relative to other sites despite similar in-situ estimates of PV-FC. Biome-specific assumptions likely explain this large difference in MODIS FAPAR, particularly those related to vegetation structure and parameters (e.g. leaf/soil scattering properties) that have been tuned to fit in-situ observations at field sites assigned to each biome type. The SPOT-VEG product also exhibited a sensitivity to biome-type, perhaps due to the fusion of MODIS and CYCLOPES products to generate the SPOT-VEG GEOV1 product.

The sensitivity to biome type is broadly consistent with previous FAPAR product comparisons in other regions of the world. McCallum et al. (2010) identified poor consistency within needle-leaf and mixed forests, ostensibly bearing little relevance to Australian forests classified as broadleaf evergreen (MDC12Q1). However, Australian forests have unique features that defy easy inclusion within existing global vegetation classifications. Changes in surface conditions, tree density and forest floor conditions (e.g. understory vegetation) that impact high-latitude forests (Kobayashi, Suzuki, & Kobayashi, 2007; McCallum et al., 2010) may also be relevant to Australian forests. McCallum et al. (2010) identified a high level of consistency in cropland regions between MODIS and MERIS, in particular with regard to seasonality. A relatively high level of seasonal consistency within managed (or agricultural) land (not shown) between the two products was identified here. Within woody savanna of northern Australia, Kanniah, Beringer, Hutley, Tapper, and Zhu (2009) identified increased consistency of MODIS LAI/FAPAR products with in-situ measurements during the Australian dry season. This increased consistency was linked to the absence of significant understory green vegetation, leaving the overlying evergreen woody vegetation as the sole vegetation layer. During the wet season, there are two distinct vegetation layers within the woody savannas.

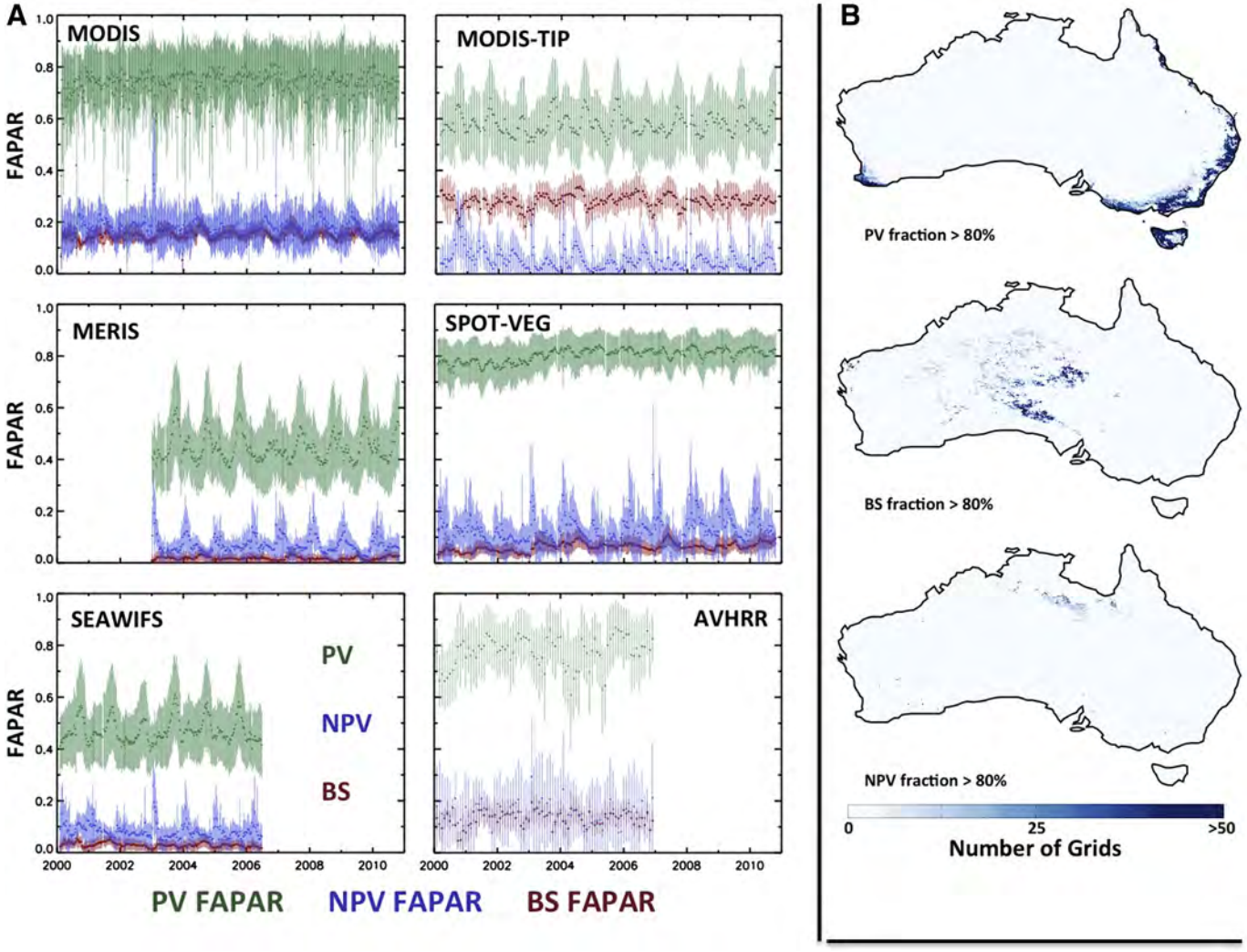

Fig. 7. A: The time-series of mean FAPAR estimates from each FAPAR product in regions predominantly consisting of PV fractional coverage, NPV fractional coverage and BS fractional coverage. B: The number of grids (scaled to [0, >50]) in the SD-FC product time-series (2000–2010) identified as predominantly consisting of PV/NPV/BS (>80% fractional cover).

Table 5
Uncertainty estimates of the FAPAR products based on published comparisons to in-situ observations.

FAPAR product	Citation	Uncertainty/bias	Field site location	Field site description
MODIS	Fensholt et al. (2004)	~0.2	W Africa (Senegal)	Semi-arid grassland and savanna (Sahel)
	Huemmrich et al. (2005)	~0.2	S Africa (W Zambia)	Kalahari woodland
	Steinberg, Goetz, and Hyer, (2006)	0.05–0.4	Central Alaska	Boreal Forest
MERIS	Gobron, Pinty, Taberner, et al. (2006),Gobron, Pinty, Aussedat, et al., 2006; Gobron et al., 2008)	0.1	Various	Various (grassland/savanna, forest, cropland)
SeaWiFS	Gobron, Pinty, Aussedat, et al. (2006)	0.1	Various	Various (grassland/savanna, forest, cropland)
MODIS-TIP (STD)	Pinty, Jung, et al. (2011)	0.15	Central Germany	Deciduous European forest
SPOT-VEG	Camacho, Cernicharo, Lacaze, Baret, and Weiss (2013)	0.1	Not specified	Not specified
AVHRR	Not available (N/A)	N/A	N/A	N/A

A result consistent with previous studies (McCallum et al., 2010; Pinty et al., 2008; Seixas et al., 2009) is a systematic difference between the MODIS and MERIS/SeaWiFS FAPAR products, identified here as a result of both a systematic offset in base-level FAPAR and sensitivity to biome type. Pinty et al. (2008) found that MODIS significantly overestimated FAPAR relative to MERIS/SeaWiFS and MODIS-TIP at two forested sites (needle-leaf evergreen, needle-leaf deciduous) that experience snow cover during the northern-hemisphere winter. MODIS was not found to overestimate FAPAR at an additional forest site (broadleaf deciduous). A SPOT-VEG derived product using the same algorithm as the MERIS product included in this study was also found to routinely underestimate FAPAR relative to the SPOT-VEG GEOV1 product (Meroni et al., 2012). This suggests that perhaps the algorithms employed rather than differences in instrumentation have greater influence on the degree of dissimilarity between products. Supporting this argument is the high level of agreement between the MERIS and SeaWiFS products observed here and elsewhere (Gobron, Belward, Pinty, & Knorr, 2010; Gobron, Pinty, Taberner, et al., 2006). Both products are based on the same algorithm but use sensor-specific parameter tuning.

5. Summary and conclusions

The evaluation of six global FAPAR satellite products across Australia highlights significant disagreement amongst the products, albeit displaying robust spatial and temporal patterns. These disagreements are spatially heterogeneous, resulting in no single product identified routinely as an outlier. These disagreements also result in differences in seasonal variation.

The findings in this study can be summarized as follows:

- Systematic differences in (1) base-level FAPAR estimates and (2) FAPAR sensitivity to spatio-temporal changes in vegetation cover are the main features of the differences between the FAPAR products.
- Differences in FAPAR sensitivity to increases in vegetation cover can be attributed in part to changes in biome type (and model assumptions therein) but are also likely related to other factors such as the assumed scattering properties of vegetation in the NIR.
- Differences between products depend on biome type, particularly if systematic differences in base-level FAPAR are accounted for. Relatively high agreement across the products occurs within savanna/grassland, shrubland and managed land (agricultural land) classified biomes. Particularly high disagreement occurs within forest-classified biomes.
- Differences between products that depend on biome type are apparent at the large-scale, when compared to the SD-FC product or using a stratification model defining different vegetation types. Such differences are consistent at the small-scale, when compared to in-situ estimated vegetation fractional (FC-dataset).
- A comparison between satellite-derived FAPAR and in-situ estimated vegetation fractional cover reveals a relationship <1:1 for all FAPAR satellite products. Reasons for this can be attributed to:

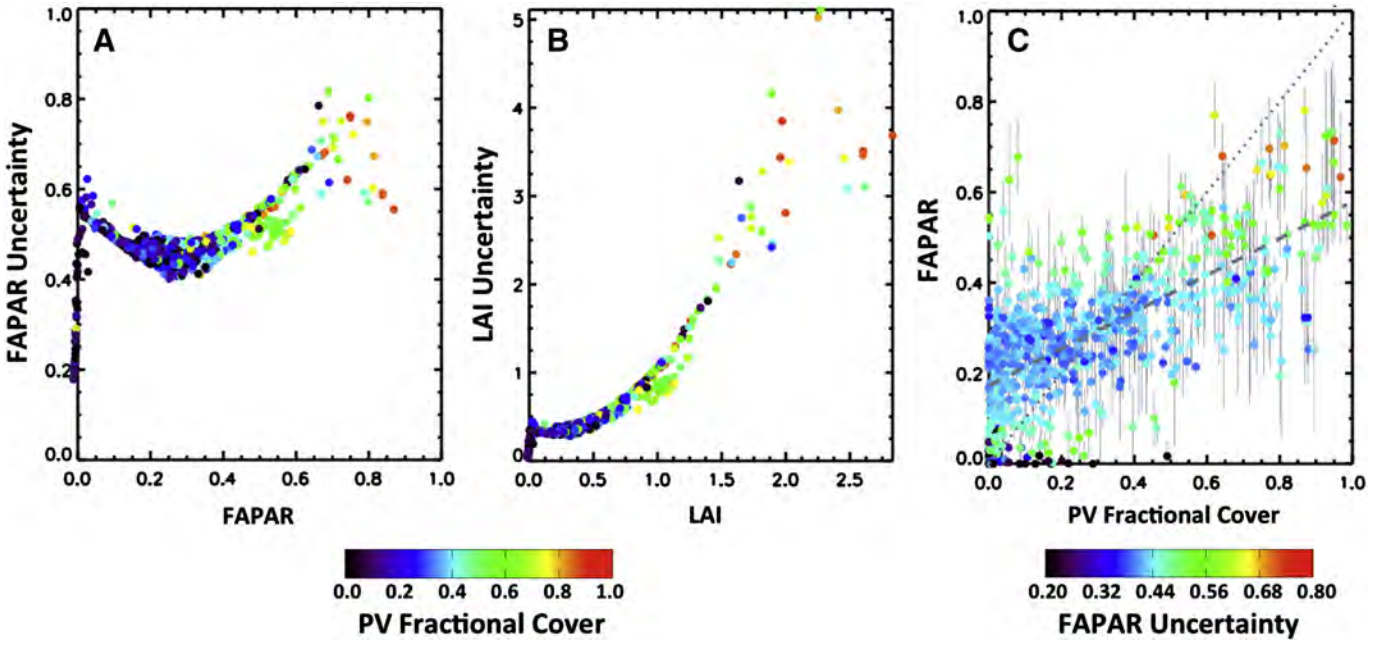

Fig. 8. A: Relationship between MODIS-TIP FAPAR and the a posteriori uncertainty in FAPAR (1.σ). PV-FC indicated by the colour scale. B: Relationship between MODIS-TIP effective LAI and the a posteriori uncertainty in effective LAI (1.σ). PV-FC indicated by the colour scale. C: Relationship between MODIS-TIP FAPAR and PV-FC. A posteriori uncertainties in FAPAR (1.σ) indicated by colour scale.

* Sensitivity in the assumed NIR scattering properties of vegetation
* Departures from the collinearity in background albedo (reflectance) in the VIS and NIR spectrums
* Lack of consistency between the definitions of FAPAR as it applies to each satellite product and the estimation of in-situ fractional cover
* Physiological characteristics (and changes) in vegetation (such as stress-induced changes) that impact the observed NIR scattering signal generated by vegetation but may not be apparent when making in-situ field estimates.

Acknowledgements

The authors would like to acknowledge the Australian Climate Change Science Program (ACCSP) for supporting this work. ACCSP is a programme of the Commonwealth Science and Industrial Research Organisation (CSIRO), the Bureau of Meteorology and the Department of Climate Change and Energy Efficiency. The Office of the Chief Executive (CSIRO) also provided financial support in the form of a post-doctoral fellowship.

The authors would like to acknowledge the custodians of the field data of fractional cover used in this study.

We acknowledge the use of the SLATS field data obtained from the Queensland State Government (Department of Environment and Resource Management) and that our study is:

"Based on or contains data provided by the State of Queensland (Department of Environment and Resource Management) [2010]. In consideration of the State permitting use of this data you acknowledge and agree that the State gives no warranty in relation to the data (including accuracy, reliability, completeness, currency or suitability) and accepts no liability (including without limitation, liability in negligence) for any loss, damage or costs (including consequential damage) relating to any use of the data. Data must not be used for direct marketing or be used in breach of the privacy laws."

We acknowledge the use of the Australian ground cover reference sites database:

ABARES (2012) Ground cover reference sites database. Australian Bureau of Agricultural and Resource Economics and Sciences, Canberra, Australia. https://rs.nci.org.au/FcSiteData/

We further acknowledge the Australian state government agencies providing support in the collection of field data contributing to the Australian ground cover reference sites database

The authors would also like to acknowledge the assistance provided by Dr. Juan-Pablo Guerschman (CSIRO–L&W), Dr. Peter Scarth (Univ. Queensland) and Ms. Jasmine Rickards (ABARES).

The authors would like to acknowledge the provision of the MODIS and AVHRR FAPAR and satellite-derived fractional cover satellite products used in this study. These datasets, and associated processing, were provided by:

The AusCover Facility, Terrestrial Ecosystem Research Network http://data.auscover.org.au/

Paget and King (2008) MODIS Land data sets for the Australian region. CSIRO Marine and Atmospheric Research Internal Report No. 004. https://lpdaac.usgs.gov/lpdaac/products/modis_policies

The authors would like to acknowledge the provision of the MERIS, SeaWiFS and MODIS-TIP FAPAR products used in this study. We acknowledge the Joint Research Center of the European Commission (EC–JRC–2011). These datasets, and associated processing, were provided by:

The SOLO (Action 24004) of EC-IES using the Joint Research Center processing chain for SeaWiFS and the European Space Grid On Demand Facility (http://gpod.eo.esa.int/) for MERIS, respectively. EC–JRC–2011: http://fapar.jrc.ec.europa.eu/

In regard to the SeaWiFS data:

"The data were possible thanks to the SeaWiFS Project (Code 970.2) and the Goddard Earth Sciences Data and Information Services Center/Distributed Active Archive Center (Code 902) at the Goddard Space Flight Center, Greenbelt, MD 20771, for the production and distribution of these data, respectively. These activities are sponsored by NASA's Earth Science Enterprise.

All SeaWiFS scenes (full resolution Local Area Coverage images and sub-sampled Global Area Coverage images) covering the study area have been processed and subsequently mapped with a nearest neighbor technique on a 2-km resolution regular grid, as explained in Mélin, Steinich, Gobron, Pinty, and Verstraete, (2002)."

The authors would like to acknowledge the provision of the SPOT-VEG FAPAR product used in this study:

"The research leading to these results has received funding from the European Community's Seventh Framework Program (FP7/2007–2013) under grant agreement no 218795. These products are the joint property of INRA, CNES, and VITO under copyright geoland2. They are generated from the SPOT VEGETATION data under copyright CNES and distribution by VITO."

The authors acknowledge the GeoLand2 data portal for access to the SPOT-VEG FAPAR product: http://www.geoland2.eu/ and the assistance provided by the GeoLand2 helpdesk.

Appendix A

In-situ estimates of vegetation fractional cover have been obtained at ~600 field sites across Australia (Fig. 1A). The fractional cover dataset consists of ~800 separate estimates. Each field site measures approximately 100 m × 100 m (1 ha), within which fractional cover estimates at three vegetation levels are obtained. The sampling strategy (Muir et al., 2011; Rickards, Stewart, Randall, & Bordas, 2012) consists of determining the presence/absence of either PV, NPV or BS along a transect at 1 m intervals for each vegetation level. Eight transects are defined in a symmetric star orientation radiating out from the centre of the field site. The ratio between the total counts of PV, NPV and BS respectively and the total number of samples taken represents the fractional cover of PV, NPV and BS for each vegetation level at the field site.

The FC estimates from the three vegetation levels must be combined to estimate the total exposed PV/NPV/BS fractional cover apparent from above the canopy. The exposed fraction is calculated by scaling the fractional cover estimates at a particular vegetation level by the 'uncovered fraction' of the vegetation level(s) above. The exposed fractional cover of PV/NPV/BS at each level and the total PV/NPV/BS fractional cover for the site ($FC_{E,i}$) are calculated as follows:

Over-story	Mid-story	Ground-cover:
$FC_{eff,i,L3} = FC_{i,\,L3}$	$FC_{eff,i,L2} = FC_{i,L2} \cdot (1 - F_{T,L3})$	$FC_{eff,i,L1} = FC_{i,L1} \cdot (1 - F_{T,L3}) \cdot (1 - F_{T,L2})$
$FC_{T,L3} = \sum_{i=1}^{2} FC_{i,L3}$	$FC_{T,L2} = \sum_{i=1}^{2} FC_{i,L2}$	
$FC_{E,i} = \sum_{L=1}^{3} FC_{eff,i,L}$		
$\sum_{i=1}^{3} FC_{E,i} = 1$		

Where:

$FC_{i,L}$	Fractional cover at level L and veg. type i
$FC_{eff,i,L}$	Effective fractional cover at level L and veg. type i
$FC_{T,L}$	Total vegetation cover (PV & NPV) at level L
L	Canopy level (1: ground cover, 2: mid-story, 3: over-story)
i	Vegetation type (1: PV, 2: NPV, 3: BS)
$FC_{E,i}$	Total exposed cover for vegetation type i

Appendix B

The split of the full FAPAR signal into the recurrent and persistent components follows algorithms developed by Donohue et al. (2009), Lu et al. (2003) and Roderick et al. (1999). The algorithm, as described by Donohue et al. (2009) is outlined as follows:

- Data dropouts (erroneous FAPAR values) are identified and removed. The difference (d_t) between a FAPAR estimate, f_t at time t, and the mean FAPAR estimate (f_m) within a 1–3 month moving window centred on time t and excluding f_t was calculated. If d_t exceeded 0.1, f_t is flagged as a dropout and replaced by f_m. A decrease of 0.1 FAPAR over one time-step is realistic if this decrease is maintained in successive time-steps. However, such a decrease followed by an equally large increase (recovery) is unrealistic and thus can be flagged as an erroneous dropout. The size of the 1–3 month moving window is dependent on the time-resolution of the satellite data.
- A 7-month moving minimum is applied to the FAPAR time-series with the FAPAR dropouts removed (F_{p1}).
- A 9-month moving average is applied to the F_{p1} time-series (F_{p2}).
- A preliminary recurrent component is calculated:

$$F_{r1} = F_t - F_{p2}$$

- The following condition is then applied to obtain the persistent FAPAR component:

$$\text{If } F_{r1} < 0, \text{ then } F_p = F_{p2} - |F_{r1}|$$

$$\text{If } F_{r1} > 0, \text{ then } F_p = F_{p2}$$

- F_p represents the final persistent component. The final recurrent component is calculated from the original time-series (F_t, dropouts removed) as follows:

$$F_r = F_t - F_p$$

Annual and seasonal climatologies of all FAPAR products (and persistent/recurrent components) were generated. Climatologies over a common time-period for all products (2003–2006) were also calculated and compared, with little difference identified between the two sets of climatologies.

Appendix C

The theoretical relationship between FAPAR and PV-FC was derived by simulating both quantities using the CanSPART radiative transfer model (Haverd et al., 2012; Lovell et al., 2012): a model of gap probability (including canopy structure effects), coupled to a modified two-stream radiative transfer scheme. CANSPART has been widely tested against other canopy structure models and above-canopy reflectances (Haverd et al., 2012), and against ground-based LIDAR observations of gap probability (Lovell et al., 2012). The range of sensitivities was obtained as the range from simulations representing extreme vegetation structure (unclumped to highly clumped) and leaf scattering coefficients. Specifically, simulations were performed for leaf area indices ranging from 0.2 to 5 with: (i) intermediate clumping (790 stems ha-1); (ii) high clumping (200 stems ha-1); (iii) no clumping (horizontally homogeneous vegetation) and (iv) extreme values (+2 s.d.) of leaf scattering coefficients; and (v) vertical leaf angle distribution (instead of spherical). Mean leaf scattering coefficients and their variability were derived from an ensemble of 50 PROSPECT (Jacquemoud & Baret, 1990) simulations for Eucalyptus leaves, with input parameter values randomly drawn from samples with mean and standard deviation derived from literature values (Barry, Newnham, & Stone, 2009; Datt, 1998, 1999).

References

Bacour, C., Baret, F., Beal, D., Weiss, M., & Pavageau, K. (2006). Neural network estimation of LAI, fAPAR, fCover and LAI x C_{ab}, from top of canopy MERIS reflectance data: Principles and validation. *Remote Sensing of Environment*, *105*(4), 313–325.

Baret, F., Hagolle, O., Geiger, B., Bicheron, P., Miras, B., Huc, M., et al. (2007). LAI, fAPAR and fCover CYCLOPES global products derived from VEGETATION: Part 1: Principles of the algorithm. *Remote Sensing of Environment*, *110*(3), 275–286.

Baret, F., Weiss, M., Lacaze, R., Camacho, F., Makhamara, H., Pacholcyzk, P., & Smets, B. (2013). GEOV1: LAI and FAPAR essential climate variables and FCOVER global time-series capitalizing over existing products. Part 1: Principles of development and production. *Remote Sensing of Environment*, *137*, 299–309.

Barry, K. M., Newnham, G. J., & Stone, C. (2009). Estimation of chlorophyll content in *eucalyptus globulus* foliage with the leaf reflectance model PROSPECT. *Agricultural and Forest Meteorology*, *149*(6), 1209–1213.

Boening, C., Willis, J. K., Landerer, F. W., Nerem, R. S., & Fasullo, J. (2012). The 2011 La Nina: So strong, the oceans fell. *Geophysical Research Letters*, *39*, L19602.

Camacho, F., Cernicharo, J., Lacaze, R., Baret, F., & Weiss, M. (2013). GEOV1: LAI, FAPAR essential climate variables and FCOVER global time-series capitalizing over existing products. Part 2: Validation and intercomparison with reference products. *Remote Sensing of Environment*, *37*, 310–329.

Chi, H. (2003). Practical atmospheric correction of NOAA-AVHRR data using the bare-sand soil line method. *International Journal of Remote Sensing*, *24*(17), 3369–3379.

Daniell, T. M. (2009). The implications of a decade of drought in Australia (1996–2007). *Sécheresse*, *20*(1), 171–180.

Datt, B. (1998). Remote sensing of chlorophyll a, chlorophyll b, chlorophyll a + b, and total carotenoid content in eucalyptus leaves. *Remote Sensing of Environment*, *66*(2), 111–121.

Datt, B. (1999). Remote sensing of water content in Eucalyptus leaves. *Australian Journal of Botany*, *47*(6), 909–923.

Donohue, R. J., McVicar, T. I. M., & Roderick, M. L. (2009). Climate-related trends in Australian vegetation cover as inferred from satellite observations, 1981–2006. *Global Change Biology*, *15*(4), 1025–1039.

Donohue, R. J., Roderick, M. L., & McVicar, T. R. (2008). Deriving consistent long-term vegetation information from AVHRR reflectance data using a cover-triangle-based framework. *Remote Sensing of Environment*, *112*(6), 2938–2949.

FAO (2008). Development of standards for essential climate variables: Fraction of Absorbed Photosynthetically Active Radiation (FAPAR), Version 8. Available at: http://www.fao.org/gtos/pubs.html

Fasullo, J. T., Boening, C., Landerer, F. W., & Nerem, R. S. (2013). Australia's unique influence on global sea level in 2010–2011. *Geophysical Research Letters*, *40*(1–6), http://dx.doi.org/10.1002/grl.50834.

Fensholt, R., Sandholt, I., & Rasmussen, M. S. (2004). Evaluation of MODIS LAI, fAPAR and the relation between fAPAR and NDVI in a semi-arid environment using in situ measurements. *Remote Sensing of Environment*, *91*(3), 490–507.

Field, C. B., Randerson, J. T., & Malmström, C. M. (1995). Global net primary production: Combining ecology and remote sensing. *Remote Sensing of Environment*, *51*(1), 74–88.

Fraction of absorbed photosynthetically active radiation by green vegetation. Liang, S., Li, X., & Wang, J. (Eds.). (2012). *Advanced remote sensing: Terrestrial information extraction and applications* (pp. 383–414). Oxford, UK: Elsevier Inc.

GCOS (2006). *Systematic observation requirements for satellite-based products for climate*: GCOS, 107 (90 pp.).

Gitelson, A. A., Gritz, Y., & Merzlyak, M. N. (2003). Relationships between leaf chlorophyll content and spectral reflectance and algorithms for non-destructive chlorophyll assessment in higher plant leaves. *Journal of Plant Physiology*, *160*(3), 271–282.

Gobron, N., Belward, A., Pinty, B., & Knorr, W. (2010). Monitoring biosphere vegetation 1998–2009. *Geophysical Research Letters*, *37*(15), L15402.

Gobron, N., Pinty, B., Aussedat, O., Chen, J. M., Cohen, W. B., Fensholt, R., et al. (2006b). Evaluation of fraction of absorbed photosynthetically active radiation products for different canopy radiation transfer regimes: Methodology and results using joint research center products derived from SeaWIFS against ground-based estimations. *Journal of Geophysical Research*, *111*(D13), D13110.

Gobron, N., Pinty, B., Aussedat, O., Taberner, M., Faber, O., Mélin, F., et al. (2008). Uncertainty estimates for the FAPAR operational products derived from MERIS — Impact of top-of-atmosphere radiance uncertainties and validation with field data. *Remote Sensing of Environment*, *112*(4), 1871–1883.

Gobron, N., Pinty, B., Mélin, F., Taberner, M., Verstraete, M. M., Robustelli, M., et al. (2007). Evaluation of the MERIS/ENVISAT FAPAR product. *Advances in Space Research*, *39*(1), 105–115.

Gobron, N., Pinty, B., Taberner, M., Mélin, F., Verstraete, M. M., & Widlowski, J. L. (2006a). Monitoring the photosynthetic activity of vegetation from remote sensing data. *Advances in Space Research*, *38*(10), 2196–2202.

Gobron, N., Pinty, B., Verstraete, M. M., & Govaerts, Y. (1997). A semidiscrete model for the scattering of light by vegetation. *Journal of Geophysical Research-Atmospheres*, *102*(D8), 9431–9446.

Gobron, N., Pinty, B., Verstraete, M., & Govaerts, Y. (1999). The MERIS global vegetation index (MGVI): Description and preliminary application. *International Journal of Remote Sensing*, *20*(9), 1917–1927.

Gobron, N., Pinty, B., Verstraete, M. M., & Taberneret, M. (2002). VEGETATION, an optimised FAPAR algorithm theoretical basis document. *JRC Publication EUR 20146 EN*. Luxembourg, UK: Publication Office European Union.

Gobron, N., Pinty, B., Verstraete, M. M., & Widlowski, J. L. (2000). Advanced vegetation indices optimized for up-coming sensors: Design, performance, and applications. *IEEE Transactions on Geoscience and Remote Sensing*, *38*(6), 2489–2505.

Guerschman, J. P., Hill, M. J., Renzullo, L. J., Barrett, D. J., Marks, A. S., & Botha, E. J. (2009). Estimating fractional cover of photosynthetic vegetation, non-photosynthetic vegetation and bare soil in the Australian tropical savanna region upscaling the EO-1 hyperion and MODIS sensors. *Remote Sensing of Environment*, *113*(5), 928–945.

Haverd, V., Lovell, J. L., Cuntz, M., Jupp, D. L. B., Newnham, G. J., & Sea, W. (2012). The Canopy Semi-analytic P_{gap} And Radiative Transfer (CanSPART) model: Formulation and application. *Agricultural and Forest Meteorology*, *160*, 14–35.

Haverd, V., Raupach, M. R., Briggs, P. R., Canadell, J. G., Isaac, P., Pickett-Heaps, C., et al. (2013). Multiple observation types reduce uncertainty in Australia's terrestrial carbon and water cycles. *Biogeosciences*, *10*, 2011–2040.

Huemmrich, K. F., Privette, J. L., Mukelabai, M., Myneni, R. B., & Knyazikhin, Y. (2005). Time-series validation of MODIS land biophysical products in a Kalahari woodland, Africa. *International Journal of Remote Sensing*, *26*(19), 4381–4398.

Jacquemoud, S., & Baret, F. (1990). PROSPECT: A model of leaf optical properties spectra. *Remote Sensing of Environment*, *34*(2), 75–91.

Jung, M., Verstraete, M., Gobron, N., Reichstein, M., Papale, D., Bondeau, A., et al. (2008). Diagnostic assessment of European gross primary production. *Global Change Biology*, *14*(10), 2349–2364.

Kaminski, T., Knorr, W., Scholze, M., Gobron, N., Pinty, B., Giering, R., et al. (2012). Consistent assimilation of MERIS FAPAR and atmospheric CO_2 into a terrestrial vegetation model and interactive mission benefit analysis. *Biogeosciences*, *9*(8), 3173–3184.

Kanniah, K. D., Beringer, J., Hutley, L. B., Tapper, N. J., & Zhu, X. (2009). Evaluation of collections 4 and 5 of the MODIS gross primary productivity product and algorithm improvement at a tropical savanna site in northern Australia. *Remote Sensing of Environment*, *113*(9), 1808–1822.

Kilinc, M., Beringer, J., Hutley, L. B., Haverd, V., & Tapper, N. (2012). An analysis of the surface energy budget above the world's tallest angiosperm forest. *Agricultural and Forest Meteorology*, *166*, 23–31.

Knorr, W., Kaminski, T., Scholze, M., Gobron, N., Pinty, B., Giering, R., et al. (2010). Carbon cycle data assimilation with a generic phenology model. *Journal of Geophysical Research: Biogeosciences*, *115*(G4), 2005–2012.

Knyazikhin, Y., Glassy, J., Privette, J. L., Tian, Y., Lotsch, A., Zhang, Y., et al. (1999). *MODIS leaf area index (LAI) and fraction of photosynthetically active radiation absorbed by vegetation (FPAR) product (MOD15) algorithm theoretical basis document.* Theoretical basis document. Greenbelt, MD, 20771: NASA Goddard Space Flight Center.

Knyazikhin, Y., Martonchik, J. V., Myneni, R. B., Diner, D. J., & Running, S. W. (1998). Synergistic algorithm for estimating vegetation canopy leaf area index and fraction of absorbed photosynthetically active radiation from MODIS and MISR data. *Journal of Geophysical Research*, *103*(D24), 32257–32276.

Kobayashi, H., Suzuki, R., & Kobayashi, S. (2007). Reflectance seasonality and its relation to the canopy leaf area index in an Eastern Siberian larch forest: Multi-satellite data and radiative transfer analyses. *Remote Sensing of Environment*, *106*(2), 238–252.

Leuning, R., Cleugh, H. A., Zegelin, S. J., & Hughes, D. (2005). Carbon and water fluxes over a temperate Eucalyptus forest and a tropical wet/dry savanna in Australia: Measurements and comparison with MODIS remote sensing estimates. *Agricultural and Forest Meteorology*, *129*, 151–173.

Lovell, J. L., Haverd, V., Jupp, D. L. B., & Newnham, G. J. (2012). The Canopy Semi-Analytic P_{Gap} And Radiative Transfer (CanSPART) model. Part 2. Validation using ground-based LIDAR. *Agricultural and Forest Meteorology*, *158*, 1–12.

Lu, H., Raupach, M. R., McVicar, T. R., & Barrett, D. J. (2003). Decomposition of vegetation cover into woody and herbaceous components using AVHRR NDVI time series. *Remote Sensing of Environment*, *86*(1), 1–18.

McCallum, I., Wagner, W., Schmullius, C., Shvidenko, A., Obersteiner, M., Fritz, S., et al. (2010). Comparison of four global FAPAR datasets over Northern Eurasia for the year 2000. *Remote Sensing of Environment*, *114*(5), 941–949.

McGrath, G. S., Sadler, R., Fleming, K., Tregoning, P., Hinz, C., & Veneklaas, E. J. (2012). Tropical cyclones and the ecohydrology of Australia's recent continental-scale drought. *Geophysical Research Letters*, *39*(3), L03404.

Meroni, M., Atzberger, C., Vancutsem, C., Gobron, N., Baret, F., Lacaze, R., et al. (2012). Evaluation of agreement between space remote sensing SPOT-VEGETATION fAPAR time series. *IEEE Transactions on Geoscience and Remote Sensing*, *51*(4), 1951–1962.

Mélin, F., Steinich, C., Gobron, N., Pinty, B., & Verstraete, M. M. (2002). Optimal merging of LAC and GAC data from SeaWiFS. *International Journal of Remote Sensing*, *23*(4), 801–807.

Muir, J., Schmidt, M., Tindall, D., Trevithick, R., Scarth, P., & Stewart, J. B. (2011). *Field measurement of fractional ground cover: a technical handbook supporting ground cover monitoring for Australia.* Canberra: Queensland Department of Environment and Resource Management for the Australian Bureau of Agricultural and Resource Economics and Sciences (Available at: http://adl.brs.gov.au/data/warehouse/pe_hbgcm9abll07701/HndbkGrndCovMontring2011_1.0.0_LR.pdf)

Murphy, B. F., & Timbal, B. (2008). A review of recent climate variability and climate change in southeastern Australia. *International Journal of Climatology*, *28*(7), 859–879.

Myneni, R. B., Hoffman, S., Knyazikhin, Y., Privette, J. L., Glassy, J., Tian, Y., et al. (2002). Global products of vegetation leaf area and fraction absorbed PAR from year one of MODIS data. *Remote Sensing of Environment*, *83*(1), 214–231.

Myneni, B., Nemani, R. R., & Running, S. (1997). Estimation of global leaf area index and absorbed PAR using radiative transfer models. *IEEE Transactions on Geoscience and Remote Sensing*, *35*(6), 1380–1393.

Myneni, R. B., & Williams, D. L. (1994). On the relationship between FAPAR and NDVI. *Remote Sensing of Environment*, *49*(3), 200–211.

National Climate Centre, Bureau of Meteorology (2012). Australia's wettest two-year period on record: 2010-2011. *Special Climate Statement, 38* available at: http://www.bom.gov.au/climate/current/statements/scs38.pdf.

NLWRA: National Land and Water Resources Audit (2000). *Australian Agriculture Assessment 2000.* Canberra, Australia: Commonwealth of Australia (160 pp.).

NLWRA: National Land and Water Resources Audit (2001). *Australian Agriculture Assessment 2001.* Canberra, Australia: Commonwealth of Australia (480 pp.).

NVIS: Australia's native vegetation (2007). *A summary of Australia's major vegetation groups*: Department of Sustainability, Environment, Water, Population and Communities, Commonwealth of Australia, 42.

Paget, M. J., & King, E. A. (2008). MODIS land data sets for the Australian region. *CSIRO Marine and Atmospheric Research Internal Report No. 004* available at: https://remote-sensing.nci.org.au/u39/public/html/modis/lpdaac-mosaics-cmar/doc/ModisLand_PagetKing_20081203-final.pdf.

Pinty, B., Andredakis, I., Clerici, M., Kaminski, T., Taberner, M., Verstraete, M. M., et al. (2011a). Exploiting the MODIS albedos with the two-stream inversion package (JRC-TIP): 1. Effective leaf area index, vegetation, and soil properties. *Journal of Geophysical Research*, *116*(D9), D09105.

Pinty, B., Clerici, M., Andredakis, I., Kaminski, T., Taberner, M., Verstraete, M. M., et al. (2011b). Exploiting the MODIS albedos with the two-stream inversion package (JRC-TIP): 2. Fractions of transmitted and absorbed fluxes in the vegetation and soil layers. *Journal of Geophysical Research*, *116*(D9), D09106.

Pinty, B., Jung, M., Kaminski, T., Lavergne, T., Mund, M., Plummer, S., et al. (2011c). Evaluation of the JRC-TIP 0.01 products over a mid-latitude deciduous forest site. *Remote Sensing of Environment*, *115*(12), 3567–3581.

Pinty, B., Lavergne, T., Dickinson, R. E., Widlowski, J. L., Gobron, N., & Verstraete, M. M. (2006). Simplifying the interaction of land surfaces with radiation for relating remote sensing products to climate models. *Journal of Geophysical Research*, *111*(D2), D02116.

Pinty, B., Lavergne, T., Kaminski, T., Aussedat, O., Giering, R., Gobron, N., et al. (2008). Partitioning the solar radiant fluxes in forest canopies in the presence of snow. *Journal of Geophysical Research*, *113*(D4), D04104.

Pinty, B., Lavergne, T., Voßbeck, M., Kaminski, T., Aussedat, O., Giering, R., et al. (2007). Retrieving surface parameters for climate models from moderate resolution imaging spectroradiometer (MODIS)-multiangle imaging spectroradiometer (MISR) albedo products. *Journal of Geophysical Research*, *112*(D10), D10116.

Pinty, B., Lavergne, T., Widlowski, J. L., Gobron, N., & Verstraete, M. M. (2009). On the need to observe vegetation canopies in the near-infrared to estimate visible light absorption. *Remote Sensing of Environment*, *113*(1), 10–23.

Potter, C. S., Randerson, J. T., Field, C. B., Matson, P. A., Vitousek, P.M., Mooney, H. A., et al. (1993). Terrestrial ecosystem production: A process model based on global satellite and surface data. *Global Biogeochemical Cycles*, *7*(4), 811–841.

Rickards, J., Stewart, J., Randall, L., & Bordas, V. (2012). *Australian ground cover reference sites database: User guide for postGIS*: Australian Bureau of Agricultural and Resource Economics and Sciences (ABARES), Department of Agriculture, Fisheries and Forestry, Commonwealth of Australia.

Roderick, M. L., Noble, I. R., & Cridland, S. W. (1999). Estimating woody and herbaceous vegetation cover from time series satellite observations. *Global Ecology and Biogeography*, *8*(6), 501–508.

Seixas, J., Carvalhais, N., Nunes, C., & Benali, A. (2009). Comparative analysis of MODIS-FAPAR and MERIS-MGVI datasets: Potential impacts on ecosystem modeling. *Remote Sensing of Environment*, *113*(12), 2547–2559.

Sellers, P. J. (1985). Canopy reflectance, photosynthesis and transpiration. *International Journal of Remote Sensing*, *6*(8), 1335–1372.

Sellers, P. J. (1987). Canopy reflectance, photosynthesis, and transpiration, II. The role of biophysics in the linearity of their interdependence. *Remote Sensing of Environment*, *21*(2), 143–183.

Sellers, P. J., Berry, J. A., Collatz, G. J., Field, C. B., & Hall, F. G. (1992). Canopy reflectance, photosynthesis, and transpiration. III. A reanalysis using improved leaf models and a new canopy integration scheme. *Remote Sensing of Environment*, *42*(3), 187–216.

Sellers, P. J., Dickinson, R. E., Randall, D. A., Betts, A. K., Hall, F. G., Berry, J. A., et al. (1997). Modeling the exchanges of energy, water, and carbon between continents and the atmosphere. *Science*, *275*(5299), 502–509.

Shabanov, N. V., Huang, D., Yang, W., Tan, B., Knyazikhin, Y., Myneni, R. B., Ahl, D. E., Gower, S. T., & Huete, A. R. (2005). Analysis and optimization of the MODIS leaf area index algorithm retrievals over broadleaf forests. *IEEE Transactions on Geoscience and Remote Sensing*, *43*(8), 1855–1865.

Steinberg, D. C., Goetz, S. J., & Hyer, E. J. (2006). Validation of MODIS F-PAR products in boreal forests of Alaska. *IEEE Transactions on Geoscience and Remote Sensing*, *44*(7), 1818–1828.

Tarantola, A. (2005). *Inverse problem theory and methods for model parameter estimation.* Philadelphia, PA, USA: Society for Industrial and Applied Mathematics.

Ummenhofer, C. C., England, M. H., McIntosh, P. C., Meyers, G. A., Pook, M. J., Risbey, J. S., et al. (2009). What causes southeast Australia's worst droughts? *Geophysical Research Letters*, *36*(4).

Verhoef, W. (1984). Light scattering by leaf layers with application to canopy reflectance modeling: The SAIL model. *Remote Sensing of Environment*, *16*(2), 125–141.

Vermote, E. F., Tanré, D., Deuze, J. L., Herman, M., & Morcette, J. -J. (1997). Second simulation of the satellite signal in the solar spectrum, 6S: An overview. *IEEE Transactions on Geoscience and Remote Sensing*, *35*(3), 675–686.

Widlowski, J. L., Pinty, B., Lavergne, T., Verstraete, M. M., & Gobron, N. (2005). Using 1-D models to interpret the reflectance anisotropy of 3-D canopy targets: Issues and caveats. *IEEE Transactions on Geoscience and Remote Sensing*, *43*(9), 2008–2017.